USGS
science for a changing world

Prepared in cooperation with the Eastern Nebraska Water Resource Assessment

# Evaluation of Geophysical Techniques for the Detection of Paleochannels in the Oakland Area of Eastern Nebraska as Part of the Eastern Nebraska Water Resource Assessment

Scientific Investigations Report 2011–5228

U.S. Department of the Interior
U.S. Geological Survey

**Cover.** Background: Orthophotography of the Oakland, Nebraska, study area.
Inset: Eastern Nebraska Water Resources Assessment area, April 2007. Photograph by Jesse Korus, Lower Platte South Natural Resources District, Lincoln, Nebraska.

# Evaluation of Geophysical Techniques for the Detection of Paleochannels in the Oakland Area of Eastern Nebraska as Part of the Eastern Nebraska Water Resource Assessment

By Jared D. Abraham, Paul A. Bedrosian, Theodore H. Asch, Lyndsay B. Ball, James C. Cannia, Jeffery D. Phillips, and Susan Lackey

Prepared in cooperation with the Eastern Nebraska Water Resource Assessment

Scientific Investigations Report 2011–5228

**U.S. Department of the Interior**
**U.S. Geological Survey**

**U.S. Department of the Interior**
KEN SALAZAR, Secretary

**U.S. Geological Survey**
Marcia K. McNutt, Director

U.S. Geological Survey, Reston, Virginia: 2012



Suggested citation:
Abraham, J.D., Bedrosian, P.A., Asch, T.H., Ball, L.B., Cannia, J.C., Phillips, J.D., and Lackey, Susan, 2012, Evaluation of geophysical techniques for the detection of paleochannels in the Oakland area of eastern Nebraska as part of the Eastern Nebraska Water Resource Assessment: U.S. Geological Survey Scientific Investigations Report 2011–5228, 40 p.

# Acknowledgments

The authors thank the managers of the Lewis and Clark, Lower Elkhorn, Lower Platte North, Lower Platte South, Nemaha, and Papio-Missouri Natural Resources Districts for coordination of financial and material support of this program.

# Contents

# Figures

## Tables

# Conversion Factors and Datums

SI to Inch/Pound

| Multiply | By | To obtain |
|---|---|---|
| | Length | |
| millimeter (mm) | 0.03937 | inch (in.) |
| centimeter (cm) | 0.3937 | inch (in.) |
| meter (m) | 3.281 | foot (ft) |
| kilometer (km) | 0.6214 | mile (mi) |
| | Area | |
| hectare (ha) | 2.471 | acre |
| hectare (ha) | 0.00381 | square mile ($mi^2$) |
| square meter ($m^2$) | 0.0002471 | acre |
| square kilometer ($km^2$) | 247.1 | acre |
| square meter ($m^2$) | 10.76 | square foot ($ft^2$) |
| square centimeter ($cm^2$) | 0.1550 | square inch ($ft^2$) |
| square kilometer ($km^2$) | 0.3861 | square mile ($mi^2$) |
| | Volume | |
| cubic meter ($m^3$) | 35.31 | cubic foot ($ft^3$) |
| cubic meter ($m^3$) | 1.308 | cubic yard ($yd^3$) |
| liter (L) | 0.2642 | gallon (gal) |
| | Mass | |
| gram (g) | 0.03527 | ounce, avoirdupois (oz) |
| kilogram (kg) | 2.205 | pound avoirdupois (lb) |
| | Density | |
| kilogram per cubic meter ($kg/m^3$) | 0.06242 | pound per cubic foot ($lb/ft^3$) |
| gram per cubic centimeter ($g/cm^3$) | 62.4220 | pound per cubic foot ($lb/ft^3$) |

Temperature in degrees Celsius (°C) may be converted to degrees Fahrenheit (°F) as follows:

$$°F=(1.8\times°C)+32.$$

Electrical resistivity is given in ohm-meters (ohm-m), unless otherwise specified.

Vertical coordinate information is referenced to the World Geodetic System of 1984 (WGS 84) ellipsoid, except as noted in text.

Horizontal coordinate information is referenced to the North American Datum of 1983 (NAD 83), Universal Transverse Mercator Zone 14 (UTM Zone 14), except as noted in text.

Elevation, as used in this report, refers to distance above the vertical datum.

# Abbreviations

| | |
|---|---|
| AGG | airborne gravity gradiometer |
| AMT | audio-magnetotelluric |
| CSD | Conservation and Survey Division (University of Nebraska–Lincoln) |
| EM | electromagnetic |
| ENWRA | Eastern Nebraska Water Resource Assessment |
| FDEM | frequency-domain electromagnetic |
| GPS | global positioning system |
| HEM | helicopter electromagnetic |
| MT | magnetotelluric |
| NRD | Natural Resources District |
| TDEM | time-domain electromagnetic |
| TDS | total dissolved solids |
| TE | transverse electric |
| TM | transverse magnetic |
| USGS | U.S. Geological Survey |
| UTM | Universal Transverse Mercator |

# Evaluation of Geophysical Techniques for the Detection of Paleochannels in the Oakland Area of Eastern Nebraska as Part of the Eastern Nebraska Water Resource Assessment

By Jared D. Abraham, Paul A. Bedrosian, Theodore H. Asch, Lyndsay B. Ball, James C. Cannia, Jeffery D. Phillips, and Susan Lackey

## Abstract

Over the winter and spring of 2009, the U.S. Geological Survey conducted a general assessment of the capabilities of several geophysical tools to delineate buried paleochannel aquifers in the glacial terrain of eastern Nebraska. Mapping these paleochannels is an important objective for the Eastern Nebraska Water Resources Assessment group. Previous attempts at mapping these channels included a helicopter electromagnetic survey flown over an area near the town of Oakland, Nebraska, in March 2007. This survey had limited success in imaging the paleochannels due to the restricted depth of investigation of the system in the clay-rich till overburden. The purpose of this study was to investigate whether other airborne electromagnetic or surface geophysical techniques, including audio-magnetotelluric, time-domain electromagnetic, gravity, and magnetic methods, could be used to image the paleochannels in the clay-rich tills of eastern Nebraska. This report releases the results of testing the ability of selected geophysical techniques to map aquifers in glacial deposits near the town of Oakland, Nebraska.

Surface audio-magnetotelluric and time-domain electromagnetic methods achieved sufficient depth of penetration and indicated that the paleochannel was much more complex than the original geological model. Simulated and observed gravity anomalies indicate that imaging sand and gravel aquifers near Oakland, Nebraska, would be difficult due to the complex basement density contrasts. Interpretation of the magnetic data indicates no magnetic sources from geologic units above the bedrock surface. Based upon the analysis and interpretation of the four methods evaluated, we suggest a large-scale survey using a high-powered time-domain airborne system. This is the most efficient and cost-effective path forward for the Eastern Nebraska Water Assessment group to map paleochannels that lie beneath thick clay-rich glacial tills.

## Introduction

The State of Nebraska requires annual evaluation of the river basins within the State to determine whether the water resources available exceed or meet demand. A component of this evaluation is mapping aquifer location, extent, and hydrologic connection to streams and rivers. The eastern portion of Nebraska is covered by glacial till of varying thickness (fig. 1). Constraining the location and geometry of sand- and gravel-filled paleochannels within and beneath this glacial till is of primary importance in understanding the hydrogeologic framework and developing hydrologic models of this region. The U.S. Geological Survey (USGS), in cooperation with the Eastern Nebraska Water Resources Assessment (ENWRA) organizations, evaluated surficial geophysical methods to define the deep alluvial paleochannels that are the main aquifers of this area.

Natural Resources Districts (NRDs) in eastern Nebraska, including Lewis and Clark, Lower Elkhorn, Lower Platte North, Lower Platte South, Nemaha, and Papio-Missouri River NRDs, created ENWRA to study and map the hydrogeology of their management areas. ENWRA also works in cooperation with the USGS, University of Nebraska–Conservation and Survey Division (CSD), and Nebraska Department of Natural Resources. The objectives of ENRWA are to develop a three-dimensional geologic framework and water budget for the glaciated region, which includes the eastern one-fifth of Nebraska (Korus and Divine, 2007). This region contains 70 percent of the State's population but is the most limited in terms of the State's groundwater supplies. Locally governed NRDs, charged with groundwater management in Nebraska, seek to improve their management plans in response to growing populations, hydrologic drought, and new conjunctive management laws. Because of limited groundwater resources in this region of Nebraska, improved hydrogeologic mapping

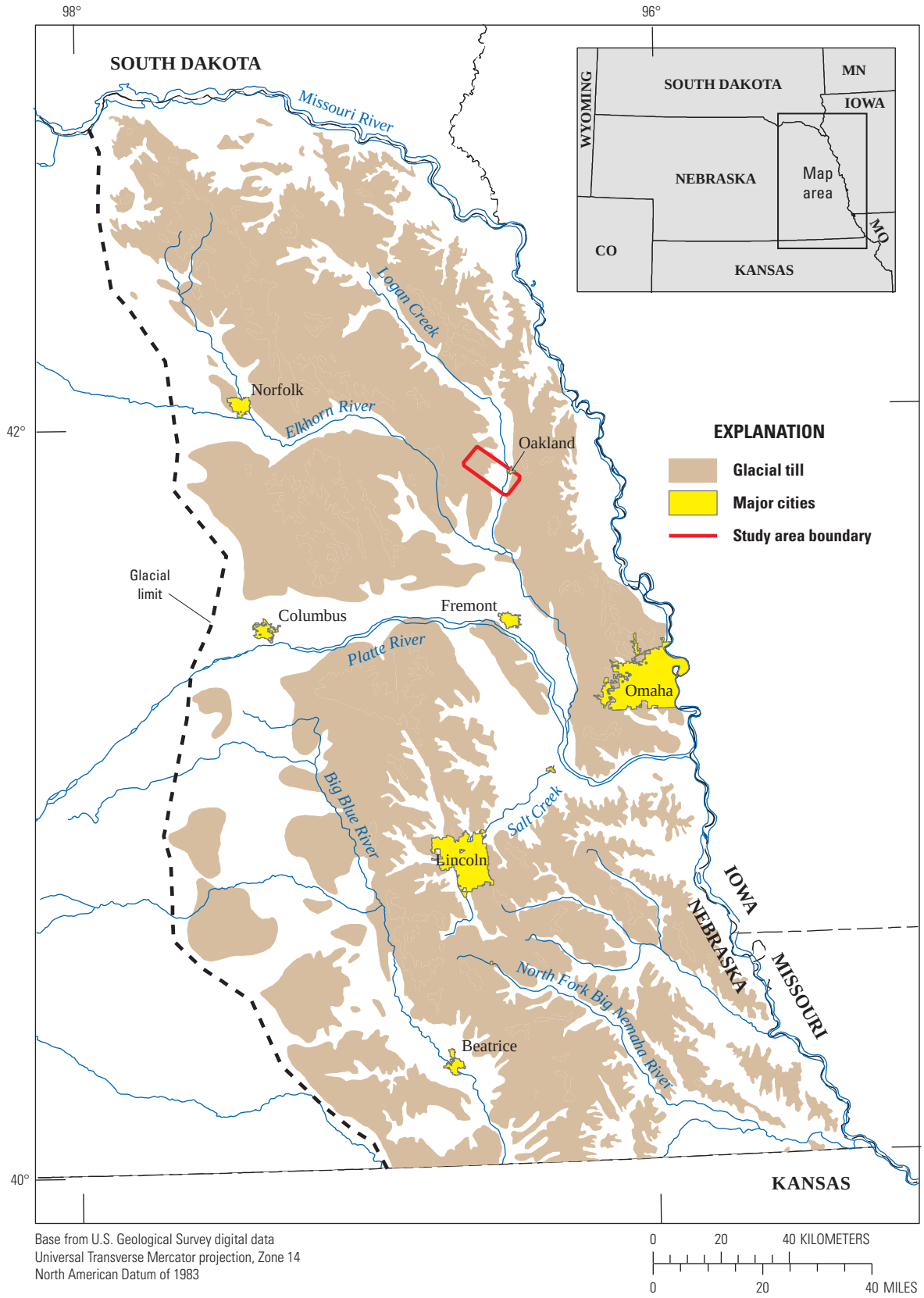


**Figure 1.** The Oakland, Nebraska, study area with respect to major rivers and areas of glacial till in eastern Nebraska. Modified from Smith and others (2008).

and characterization techniques are needed to delineate aquifers, assess their degree of hydrologic connection with streams and other aquifers, and better predict water quality and quantity. As part of the development of the hydrogeologic framework, the USGS has been cooperating with ENWRA to develop appropriate methodology and surveys to accomplish these tasks.

The USGS performed surface geophysical surveys along a 7-km transect over a presumed paleochannel in a study area west of the town of Oakland, Nebr. Seventeen test holes within the Oakland area broadly define a deep paleochannel about 5 km northwest of Oakland (fig. 2). This inferred paleochannel trends southwest to northeast and is estimated to be about 1 km wide. The objectives of the surveys were to evaluate and compare the capabilities of several geophysical methods—time-domain electromagnetic (TDEM), audio-magnetotelluric (AMT), gravity, and magnetic field—to detect and delineate this paleochannel. The Oakland area was investigated previously using helicopter electromagnetic (HEM) survey data collected in 2007 as part of the first ENWRA study (Smith and others, 2008). The HEM data were collected within a 9,324-ha area west of Oakland. The airborne geophysical system imaged the near-surface sediment; however, it was unable to image the deep alluvial paleochannels, because they are buried beneath thick clay-rich glacial tills. This report describes the evaluation of other surficial geophysical methods by the USGS to map the deeper aquifers.

## Purpose and Scope

This report presents the analysis and interpretation of data from several different geophysical methods applied at the Oakland study area (figs. 1 and 2). These methods include a combination of airborne techniques (electromagnetic (EM) and magnetic) and ground-based techniques (time-domain electromagnetic (TDEM), audio-magnetotelluric (AMT), gravity, and magnetic). This study has four major objectives: (1) to present the methodology used to evaluate the airborne geophysical data, (2) to refine the geometry of the paleochannel, (3) to evaluate the effectiveness of a range of ground-based geophysical techniques in this thick glacial-till environment, and (4) to determine the effectiveness of alternative airborne techniques in mapping hydrogeology in glaciated terrains with thick till deposits.

## Description of Study Area

The Oakland study area comprises an area of about 6.4 by 14.4 km near the town of Oakland in Burt and Cuming Counties, Nebr. (figs. 1 and 2). This site lies in the "Rolling Hills" topographic region of Nebraska (Flowerday, 1998) and within the Northeast Nebraska Glacial Drift Area, Groundwater Region 10, (Gosselin and others, 1996). This part of Nebraska is characterized by rolling, stream-dissected terrain with about 20 to 30 m of relief eroded out of thick glacial deposits overlain by multiple loess units. The site is incised by Logan Creek (fig. 2); remnant terrace deposits extend to the eastern side of the site and rolling glaciated hills extend to the west. The dominant land use is rural farm land with a mix of groundwater-irrigated and nonirrigated row-crop agriculture and pastureland. Rainfall averages about 740 mm and average annual temperatures range from –6.6 to 24.4°C (High Plains Climate Center, 2011).

### Hydrogeology

The regional aquifer primarily is composed of intermixed sand and gravel units of limited extent underlying regional glacial deposits. Depth to the regional water table ranges from 15 to 60 m, but locally perched groundwater is also present (Gosselin and others, 1996). Well yields locally can exceed 3,785 L/min, but due to limited saturated thickness of the aquifer, yields often are less than this (Nebraska Department of Natural Resources, 2009). Most registered large-capacity wells at the Oakland study area are screened in either an uplands paleochannel aquifer or in younger sand and gravel deposits present beneath Logan Creek valley and its terraces. In areas not underlain by these aquifers, locating adequate supplies of potable water can be challenging. During 2005, total groundwater withdrawals in Burt County for all public supply approximated 3.9 million L/day (Kenny and others, 2009). Some domestic and stock water supplies in the Oakland study area are provided by rural water systems such as Logan East Rural Water Systems. Wells withdraw water from the paleochannel aquifer and supply about 4,000 domestic customers east of Logan Creek.

The uppermost bedrock beneath the Oakland study area is the Cretaceous Dakota Formation (Bentall and others, l971). In this area, complex sequences of shale, siltstone, and sandstone layers with varying degrees of cementation are present (Ellis, 1984; Burchett and Smith, 1991, 1993). In upland areas, data from test holes and registered wells indicate the presence of a southwest- to northeast-trending paleochannel. The paleochannel deposit comprises 15 to 20 m of sand and gravel that historically were mapped at a coarse scale of resolution. Glacial till and multiple loess units including the Peoria, Gilman Canyon, and Loveland Loesses, along with possibly older loess units (Mason and others, 2007), overlie the sand and gravel deposits. Thicknesses of these loess units vary from less than 15 m to greater than 46 m depending on topographic position. The thickest sequences of sediments generally underlie hilltops.

Multiple episodes of erosion and deposition have occurred in Logan Creek valley. Early erosional episodes cut a channel along the west edge of the uplands. Data from test holes and registered wells indicate that this channel, along with probable subsequent channels, did not erode all of the Dakota Formation between the uplands and present day Logan Creek. Some test-hole logs (48-A-50 and 49-A-55; Burchett and Smith, 1993) indicate a bedrock high beneath the Logan Creek terrace and the presence of silt that filled much of this

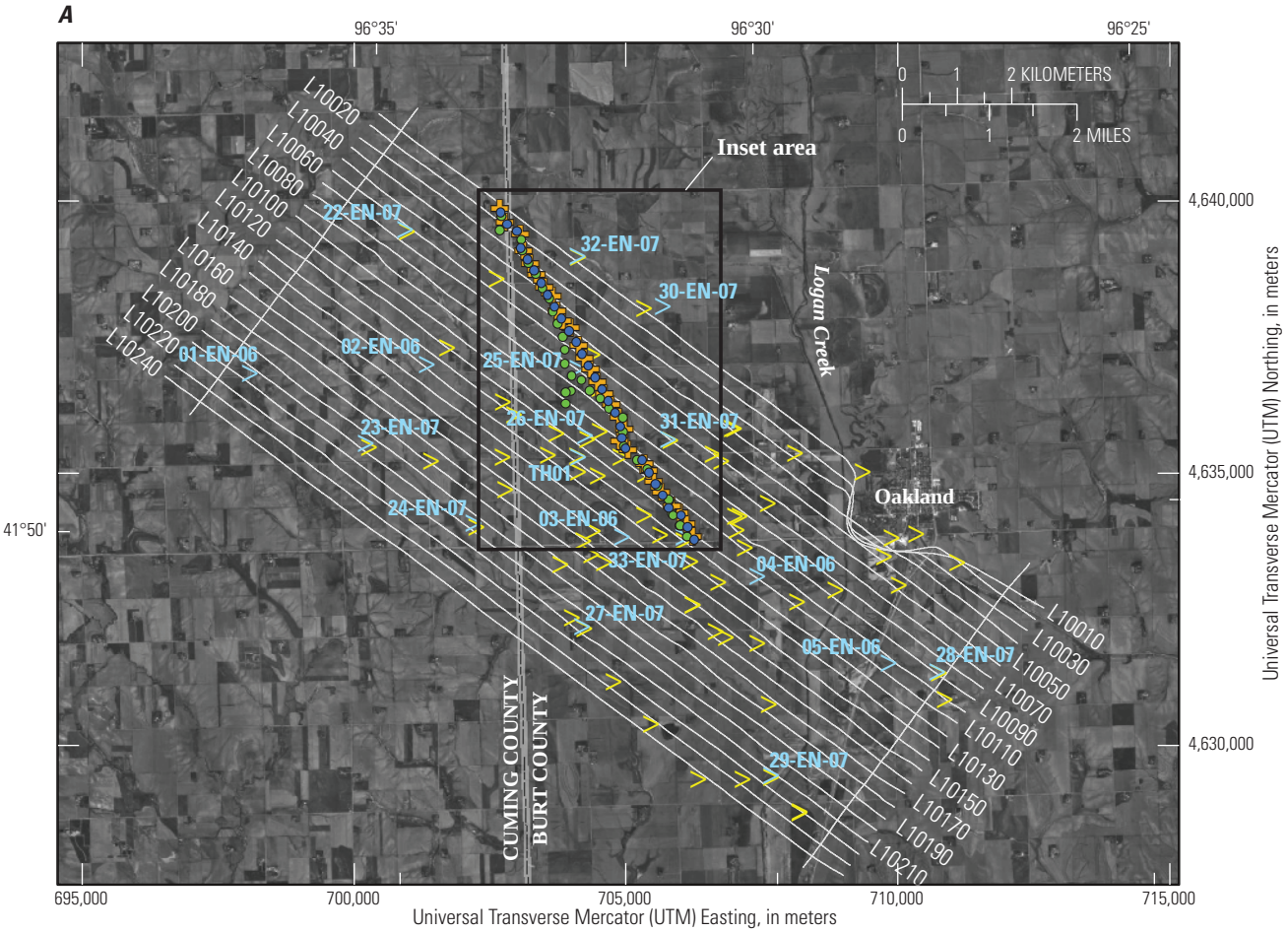


Base from U.S. Geological Survey digital orthophotography, 1999
Universal Transverse Mercator projection, Zone 14
North American Datum of 1983

**EXPLANATION**

- Gravity station
- Audio-magnetotelluric station
- Time-domain electromagnetic station
- ENWRA-drilled well
- Registered well
- Geophysical flight line

***B.*** **Inset area**

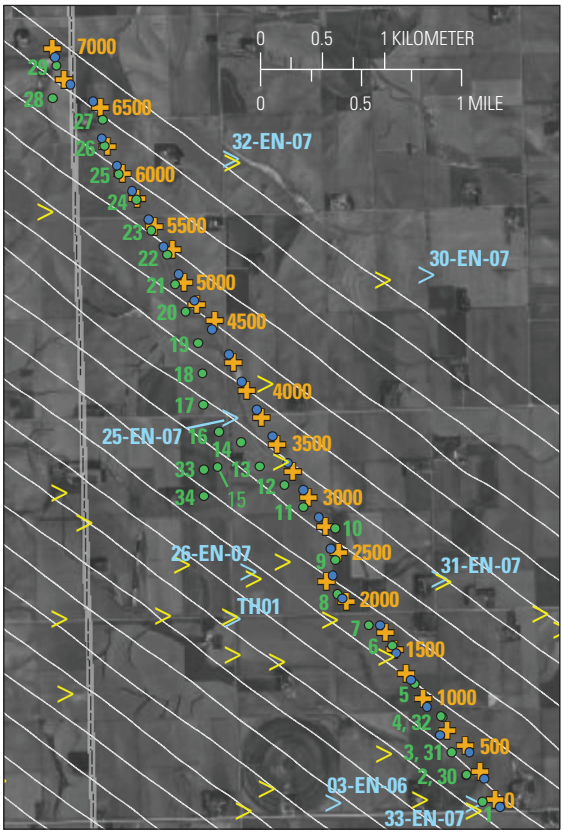


**Figure 2.** The locations of geophysical data and test holes at the Oakland, Nebraska, study area. ENWRA, Eastern Nebraska Water Resource Assessment.

channel. Later, shallow channels were eroded into these sediments and 12 to 20 m of sand or sand and gravel was deposited (test holes 48-A-50 and 47-A-50). Loveland and Peoria Loesses blanket the stream terrace with as much as 15 m of silt-size sediments.

The Dakota Formation presents a challenge for electrical resistivity interpretation because groundwater derived from this formation can have high total dissolved solids (TDS) (Bentall and others, l971). Lawton and others (1984) indicate that TDS concentrations range between 400 and 1,500 mg/L. Heavy use of high-capacity wells in the sand and gravel deposits overlying the Dakota Formation may introduce poorer quality water from the Dakota Formation into the upper aquifers used for public supply.

## Eastern Nebraska Water Resources Assessment Test-Hole Drilling

Eighteen test holes were drilled by Conservation and Survey Division (University of Nebraska–Lincoln) (CSD) with assistance from USGS and ENWRA scientists using direct rotary methods during 2006–07 and 2009 (table 1). The five test holes drilled in 2006 were located so as to target the broadest range of geologic units for use as variable control points for geophysical surveys. In 2007, test holes were concentrated in selected areas to provide additional subsurface information. Six of these test holes are within the target area for the geophysical work (fig. 2*B*). A lithologic description of sediments cut by drilling was recorded in the field, and samples were bagged at a minimum of 1.5-m intervals or at major lithologic changes. A suite of borehole geophysical logs was collected immediately after drilling, including natural gamma, resistivity, spontaneous potential, and temperature logs.

The sediments beneath the terrace are very complex. Preliminary results confirmed the presence of a bedrock high near hole 04-EN-06 (fig. 2). New lithologic data indicate the existence of a relatively steep-sided incision into this bedrock high between test holes 33-EN-07 and 03-EN-06. The bedrock surface is 15.3 m lower in hole 03-EN-06, about 1 km to the west of hole 33-EN-07. Local landowners to the south have noted this incision into the bedrock during other test-hole drilling campaigns for irrigation-well development.

Prior to the drilling program, it was conceptualized that an erosional channel on top of the Dakota Formation created a southwest- to northeast-trending paleochannel that was in-filled with sand and gravel. New data reveal a more complex geologic relation that includes an additional, deeper paleochannel trending to the east-northeast. Lithologic samples and down-hole geophysical logs indicate two sand and gravel deposits within the deeper paleochannel. The lower unit is 9.1 m thick and generally contains few silt lenses. The upper unit is 15.2 to 18.3 m thick and exhibits four depositional cycles transitioning between silt and sand and gravel.

**Table 1.** Simplified lithologic descriptions from Eastern Nebraska Water Resource Assessment (ENWRA) drilled test holes used in the geophysical investigation of the Oakland, Nebraska, study area.

[Coordinates relative to the North American Datum of 1983, Universal Transverse Mercator projection, Zone 14. Elevation relative to the World Geodetic System of 1984 ellipsoid; m, meters]

| Upper depth (meters) | Lower depth (meters) | Lithologic classification |
|---|---|---|
| Hole 01-EN-06, Cuming County, Nebraska | | |
| Easting 698090.9 m, Northing 4636801.6 m, Elevation 386.3 m | | |
| 0 | 9.1 | Silt and clay |
| 9.1 | 15.9 | Clay |
| 15.9 | 18.3 | Silt and clay |
| 18.3 | 18.9 | Sand and gravel |
| 18.9 | 22.9 | Silt and clay |
| 22.9 | 24.4 | Sand and gravel |
| 24.4 | 32.6 | Silt and clay |
| 32.6 | 37.2 | Silt and sand |
| 37.2 | 38.7 | Sand and gravel |
| 38.7 | 41.2 | Silt and clay |
| 41.2 | 47.9 | Shale |
| Hole 02-EN-06, Cuming County, Nebraska | | |
| Easting 701339.4 m, Northing 4636969.2 m, Elevation 406.3 m | | |
| 0 | 11.3 | Silt |
| 11.3 | 47.9 | Silt and clay |
| 47.9 | 61.6 | Sand and gravel |
| 61.6 | 78.3 | Shale |
| Hole 03-EN-06, Burt County, Nebraska | | |
| Easting 704936.5 m, Northing 4633794.8 m, Elevation 370.5 m | | |
| 0 | 9.8 | Silt |
| 9.8 | 30.5 | Silt and clay |
| 30.5 | 33.5 | Clay |
| 33.5 | 37.5 | Sand and gravel |
| 37.5 | 52.1 | Clay |
| 52.1 | 55.8 | Sand and gravel |
| 55.8 | 56.4 | Clay |
| 56.4 | 57.0 | Sandstone |
| 57.0 | 72.2 | Shale |
| Hole 04-EN-06, Burt County, Nebraska | | |
| Easting 707426.3 m, Northing 4633062.5 m, Elevation 364.1 m | | |
| 0 | 6.1 | Silt |
| 6.1 | 15.5 | Silt and clay |
| 15.5 | 22.3 | Silt and sand |
| 22.3 | 28.7 | Sand |
| 28.7 | 30.2 | Silt and sand |
| 30.2 | 35.1 | Clay |
| 35.1 | 35.4 | Sandstone |
| 35.4 | 54.3 | Shale |

**Table 1.** Simplified lithologic descriptions from Eastern Nebraska Water Resource Assessment (ENWRA) drilled test holes used in the geophysical investigation of the Oakland, Nebraska, study area.—Continued

[Coordinates relative to the North American Datum of 1983, Universal Transverse Mercator projection, Zone 14. Elevation relative to the World Geodetic System of 1984 ellipsoid; m, meters]

| Upper depth (meters) | Lower depth (meters) | Lithologic classification |
|---|---|---|
| Hole 05-EN-06, Burt County, Nebraska | | |
| Easting 709837.9 m, Northing 4631479.7 m, Elevation 358.5 m | | |
| 0 | 5.5 | Silt |
| 5.5 | 11.6 | Sand |
| 11.6 | 13.1 | Gravel |
| 13.1 | 48.2 | Shale |
| Hole 22-EN-07, Cuming County, Nebraska | | |
| Easting 700943.8 m, Northing 4639433.1 m, Elevation 416.6 m | | |
| 0 | 0.6 | Soil |
| 0.6 | 51.2 | Silt and clay |
| 51.2 | 67.7 | Silt and sand |
| 67.7 | 72.5 | Shale |
| Hole 23-EN-07, Cuming County, Nebraska | | |
| Easting 700220.6 m, Northing 4635511.5 m, Elevation 403.3 m | | |
| 0 | 0.6 | Soil |
| 0.6 | 42.1 | Silt and clay |
| 42.1 | 49.7 | Clay |
| 49.7 | 52.4 | Silt and sand |
| 52.4 | 68.6 | Sand and gravel |
| 68.6 | 78.6 | Shale |
| Hole 24-EN-07, Cuming County, Nebraska | | |
| Easting 702195.3 m, Northing 4634037.5 m, Elevation 382.3 m | | |
| 0 | 0.6 | Soil |
| 0.6 | 28.1 | Silt and clay |
| 28.1 | 57.0 | Sand and gravel |
| 57.0 | 66.1 | Shale |
| Hole 25-EN-07, Burt County, Nebraska | | |
| Easting 704109.9 m, Northing 4636884.0 m, Elevation 380.9 m | | |
| 0 | 0.3 | Soil |
| 0.3 | 20.1 | Silt and clay |
| 20.1 | 25.3 | Silt and sand |
| 25.3 | 36.0 | Sand |
| 36.0 | 43.3 | Sand and gravel |
| 43.3 | 45.1 | Silt and clay |
| 45.1 | 57.9 | Sand and gravel |
| 57.9 | 66.4 | Shale |
| Hole 26-EN-07, Burt County, Nebraska | | |
| Easting 704253.5 m, Northing 4635650.6 m, Elevation 388.9 m | | |
| 0 | 0.3 | Soil |
| 0.3 | 22.2 | Silt and clay |
| 22.2 | 26.8 | Silt and sand |
| 26.8 | 42.1 | Sand |
| 42.1 | 43.6 | Silt and sand |
| 43.6 | 52.7 | Sand and gravel |
| 52.7 | 62.5 | Sand |
| 62.5 | 72.5 | Shale |
| Hole 27-EN-07, Burt County, Nebraska | | |
| Easting 704197.8 m, Northing 4632146.2 m, Elevation 371.6 m | | |
| 0 | 0.6 | Soil |
| 0.6 | 42.1 | Silt and clay |
| 42.1 | 45.7 | Sand |
| 45.7 | 51.2 | Shale |
| 51.2 | 60.3 | Silt and sand[1] |
| Hole 28-EN-07, Burt County, Nebraska | | |
| Easting 710733.8 m, Northing 4631311.8 m, Elevation 378.8 m | | |
| 0 | 1.5 | Soil |
| 1.5 | 17.7 | Silt and sand |
| 17.7 | 29.9 | Silt and clay |
| 29.9 | 35.0 | Silt and sand |
| 35.0 | 41.4 | Shale |
| 41.4 | 48.8 | Sand[1] |
| 48.8 | 49.7 | Sand and gravel[1] |
| 49.7 | 54.2 | Sand[1] |
| Hole 29-EN-07, Burt County, Nebraska | | |
| Easting 707674.4 m, Northing 4629420.6 m, Elevation 354.2 m | | |
| 0 | 0.9 | Soil |
| 0.9 | 5.8 | Silt |
| 5.8 | 17.7 | Sand and gravel |
| 17.7 | 26.8 | Silt and sand |
| 26.8 | 36.0 | Shale |

**Table 1.** Simplified lithologic descriptions from Eastern Nebraska Water Resource Assessment (ENWRA) drilled test holes used in the geophysical investigation of the Oakland, Nebraska, study area.—Continued

[Coordinates relative to the North American Datum of 1983, Universal Transverse Mercator projection, Zone 14. Elevation relative to the World Geodetic System of 1984 ellipsoid; m, meters]

| Upper depth (meters) | Lower depth (meters) | Lithologic classification |
|---|---|---|
| Hole 30-EN-07, Burt County, Nebraska | | |
| Easting 705680.3 m, Northing 4638026.0 m, Elevation 383.6 m | | |
| 0 | 0.3 | Soil |
| 0.3 | 11.6 | Silt |
| 11.6 | 31.7 | Silt and clay |
| 31.7 | 35.7 | Silt and sand |
| 35.7 | 51.2 | Sand |
| 51.2 | 55.2 | Sand and gravel |
| 55.2 | 55.8 | Silt and clay |
| 55.8 | 56.4 | Silt and sand |
| 56.4 | 58.8 | Sand and gravel |
| 58.8 | 59.1 | Clay |
| 59.1 | 70.4 | Sand |
| 70.4 | 78.6 | Silt and sand |
| 78.6 | 84.7 | Shale |
| Hole 31-EN-07, Burt County, Nebraska | | |
| Easting 705783.2 m, Northing 4635595.0 m, Elevation 369.2 m | | |
| 0 | 0.3 | Soil |
| 0.3 | 17.7 | Silt and clay |
| 17.7 | 26.2 | Silt and sand |
| 26.2 | 32.0 | Silt and clay |
| 32.0 | 36.0 | Silt and sand |
| 36.0 | 40.6 | Sand |
| 40.6 | 44.2 | Silt and sand |
| 44.2 | 51.2 | Silt and clay |
| 51.2 | 51.8 | Sandstone |
| 51.8 | 54.2 | Shale |
| Hole 32-EN-07, Burt County, Nebraska | | |
| Easting 704114.4 m, Northing 4638960.3 m, Elevation 396.1 m | | |
| 0 | 0.3 | Soil |
| 0.3 | 43.9 | Silt and clay |
| 43.9 | 52.7 | Silt and sand |
| 52.7 | 65.8 | Sand |
| 65.8 | 72.5 | Shale |
| Hole 33-EN-07, Burt County, Nebraska | | |
| Easting 706061.3 m, Northing 4633787.1 m, Elevation 366.8 m | | |
| 0 | 0.6 | Soil |
| 0.6 | 28.1 | Silt and clay |
| 28.1 | 32.9 | Silt and sand |
| 32.9 | 34.5 | Silt and clay |
| 34.5 | 37.2 | Sand |
| 37.2 | 40.6 | Silt and clay |
| 40.6 | 41.1 | Sand |
| 41.1 | 47.2 | Shale |
| Hole TH01, Burt County, Nebraska | | |
| Easting 704127.7 m, Northing 4635267.6 m, Elevation 387.2 m | | |
| 0 | 0.9 | Silt |
| 0.9 | 4.6 | Silt and clay |
| 4.6 | 6.1 | Silt |
| 6.1 | 13.7 | Silt and clay |
| 13.7 | 15.2 | Clay |
| 15.2 | 16.8 | Silt |
| 16.8 | 18.3 | Silt and clay |
| 18.3 | 19.5 | Sand |
| 19.5 | 19.8 | Clay |
| 19.8 | 22.9 | Silt and clay |
| 22.9 | 24.4 | Silt and sand |
| 24.4 | 29.0 | Silt and clay |
| 29.0 | 30.5 | Sand and Clay |
| 30.5 | 32.6 | Silt and sand |
| 32.6 | 35.1 | Sand and gravel |
| 35.1 | 35.7 | Silt and sand |
| 35.7 | 41.1 | Sand and gravel |
| 41.1 | 42.7 | Gravel |
| 42.7 | 52.4 | Sand and gravel |
| 52.4 | 53.6 | Silt and clay |
| 53.6 | 54.9 | Sand |
| 54.9 | 56.4 | Silt and clay |
| 56.4 | 70.1 | Sand and gravel |
| 70.1 | 77.7 | Clay |
| 77.7 | 131.7 | Sandstone |

[1]Likely poorly lithified material within the Dakota Formation.

During drilling in 2006–07, only 6 to 18 m of the Dakota Formation was penetrated. The Dakota consisted of shale or clay, siltstone, and very fine to fine-grained sand and sandstone with many lignite lenses. The top of the Dakota Formation was often difficult to identify during field operations because the sediments were generally not well cemented and inspection without the availability of a microscope did not readily distinguish these materials from overlying sediments. Additional laboratory examination is needed to finalize the depth of this stratigraphic unit.

# Methods of Investigation

A suite of geophysical techniques have been applied at the Oakland study area (fig. 2). Helicopter electromagnetic and magnetic data were collected in a series of parallel lines and tie lines during the spring of 2007. TDEM, AMT, and gravity data were collected during the late winter and spring of 2009 along a 7-km profile across the paleochannel interpreted from test hole data. Data were processed and compared to lithologic and borehole geophysical data available from the ENWRA drilled test holes. The fundamentals of each technique applied at the Oakland study area are discussed in the following sections.

## Electrical Methods

Electromagnetic geophysical methods detect variations in the electrical properties of rocks, in particular, electrical resistivity, or its reciprocal, electrical conductivity. Electrical resistivity can be correlated with geologic units on the surface and at depth using lithologic logs to provide a three-dimensional (3-D) picture of subsurface geology. In the upper crust, the resistivities of geologic units are largely dependent upon their fluid content, pore-volume porosity, effective porosity, and conductive mineral content (Keller, 1989). Although there is not a one-to-one relation between lithology and resistivity, there are general correlations that can be made using typical values, even though values can be found at other localities that may fall outside of the ranges presented herein (Palacky, 1987). Fluids within the pore spaces and fracture openings can reduce electrical resistivities in what would otherwise be a resistive rock matrix, especially if the fluids are high in total dissolved solids. Resistivity can also be lowered by the presence of electrically conductive clay minerals, graphitic carbon, and metallic mineralization. For example, it is common for altered volcanic rocks to contain replacement minerals that have resistivities 10 times lower than those of the surrounding rocks (Nelson and Anderson, 1992). Fine-grained sediments, such as clay-rich alluvium, marine shales, and other mudstones, are normally conductive from a few ohm-meters to a few tens of ohm-meters (Keller, 1987; Palacky, 1987). Metamorphic rocks (nongraphitic) and unaltered, unfractured igneous rocks are normally moderately to highly resistive (a few hundreds to thousands of ohm-meters). Carbonate rocks can have similarly high resistivities depending on their fluid content, porosity, and impurities (Keller, 1987; Palacky, 1987). Fault zones may be moderately conductive (tens of ohm-meters) when composed of rocks fractured enough to have hosted fluid transport and consequent mineralogical alteration (Eberhart-Phillips and others, 1995). Higher subsurface temperatures cause higher ionic mobility that reduces rock resistivities (Keller, 1987; Palacky, 1987). Tables of electrical resistivity for a variety of rocks, minerals, and geological environments are in Keller (1987) and Palacky (1987).

## Helicopter Electromagnetic Method

HEM surveys have been increasingly employed to characterize groundwater aquifers and their geologic settings (Smith and others, 2008). These data can be used to map subsurface electrical and magnetic properties of the Earth that can be related to geologic and hydrologic features. One objective of the HEM survey at the Oakland study area was to define the paleochannel identified by the test-hole drilling program.

The main part of the frequency-domain electromagnetic (FDEM) geophysical system used at the Oakland study area is housed in a cylindrical tube, or "bird," that is towed beneath the helicopter. The bird contains transmitter and receiver coils that operate at different frequencies. Modern birds use five or six frequencies spanning the range from 100 hertz (Hz) to over 100 kilohertz (kHz) (Smith and others, 2008). As a general rule, lower frequencies probe deeper than higher frequencies. Because the depth of penetration depends on the electrical conductivity of the Earth layers, the frequencies used for any given survey are tailored for the local geology. The EM measurements made by the receivers—along with total magnetic field, global positioning system (GPS), altitude, and sometimes radiometric data—are sent over a power and signal cable to a processing and digital recording system in the helicopter. Discrete measurements of the geophysical data (FDEM and total field magnetic) are made approximately every 3 m along the flight line, resulting in high data density along a flight line and sparse data density across flight lines. Details on the data acquisition and processing can be found in Smith and others (2008).

Each of the HEM frequencies yields an apparent resistivity for the corresponding depth of penetration. Low frequencies penetrate a conductive Earth more than higher frequencies. For a uniform Earth, the depth of penetration of a normally incident electromagnetic wave is described by the skin depth, $\varsigma$,which is a function of frequency and Earth conductivity:

$$\varsigma = \sqrt{\frac{2}{\omega\mu\sigma}}$$

where

$\varsigma$ is skin depth [m],

$\omega$ is angular frequency [radian per second (rad/s)], also $\omega = 2\pi f$, where $f$ is frequency in Hz,

$\mu$ is magnetic permeability [Henry per meter (H/m)], and

$\sigma$ is electrical conductivity [siemens per meter (S/m)].

The skin depth is the depth at which the amplitude of the incident EM wave is attenuated to 1/*e* (about 37 percent) of its initial amplitude. This characterizes the ohmic loss of the material. Secondary (induced) fields must diffuse back through the electrically lossy material to reach the receiver coil, thereby suffering another, equivalent loss.

At the Oakland study area, a total of 385 km (239 mi) of data were collected over 26 flight lines (Smith and others, 2008). The flight-line pattern consisted of a series of narrowly spaced parallel traverse lines connected by two widely spaced tie-lines (fig. 2, table 2). The nominal frequencies of operation were 385, 1,500, 3,300, 6,200, 25,000, and 115,000 Hz (table 3). Note that the operational frequencies increase by about a factor of four. Accordingly, each successively higher frequency probes about half as deep into the Earth.

**Table 3.** Coil orientations, frequencies, and sensitivities for the helicopter electromagnetic surveys (adapted from Fugro Airborne Surveys Corporation (2007) and Smith and others (2008)).

| Coil configuration | Coil separation (meters) | Nominal frequency (hertz) | Actual frequency (hertz) | Sensitivity (parts per million) |
|---|---|---|---|---|
| Coplanar | 7.9 | 385 | 380 | 0.12 |
| Coplanar | 7.9 | 1,500 | 1,760 | 0.12 |
| Coaxial | 9.0 | 3,300 | 3,270 | 0.12 |
| Coplanar | 7.9 | 6,200 | 6,520 | 0.24 |
| Coplanar | 7.9 | 25,000 | 26,640 | 0.60 |
| Coplanar | 7.9 | 115,000 | 116,400 | 0.60 |

## Time-Domain Electromagnetic Method

The time-domain electromagnetic method (TDEM) technique is used to constrain subsurface electrical resistivity structure, typically in the depth range from 50 to 500 m. As such, it fills an important gap between near-surface techniques (for example, direct-current resistivity and capacitively coupled resistivity) and deeper techniques such as the magnetotelluric method (Sharma, 1997). For this reason it finds frequent use in hydrologic studies, especially in regions where deep hydrologic data are needed (Fitterman and Stewart, 1986; Fitterman, 1988).

TDEM is an active-source inductive electromagnetic technique that provides subsurface resistivity constraints by passing current through a relatively large, rectangular, ungrounded wire loop on the ground surface, which generates a primary magnetic field (Fitterman and Labson, 2005) according to Ampere's law. This primary current is rapidly turned off, thereby causing a change in magnetic flux that induces an electromotive force according to Faraday's law. In TDEM, secondary magnetic fields are produced by the decay of subsurface eddy and galvanic currents, and are typically measured as a voltage on a horizontal (level) receiver coil at the surface. Via Faraday's law a horizontal receiver coil senses the time rate of change of the vertical (Z) component of the magnetic field.

An apparent resistivity, $\rho_a$, can be calculated from the measured voltage. The apparent resistivity is solely a mathematical transform; however, it serves two important purposes. First, subtle differences in the measured receiver voltage due to changes in subsurface resistivity are accentuated by the power-law dependence of apparent resistivity on time and voltage. Second, the TDEM response of a homogeneous, isotropic half-space is such that the late-stage apparent resistivity is time dependent, but asymptotic to the true half-space resistivity at late times of the transient decay. For more complicated, heterogeneous Earth structure, the variation of apparent resistivity with time can be viewed as a proxy for the variation of true Earth resistivity with depth. The actual electrical resistivity distribution in the Earth is computed from the apparent resistivity via the process of inversion. Additional details on the TDEM sounding method can be found in Nabighian and Macnae (1991), Christiansen and Christensen (2003), Danielsen and others (2003), and Fitterman and Labson (2005).

TDEM data were collected at a total of 29 sites along the 7-km profile with nominal 250-m site spacing (fig. 2). Data were collected using two systems: the Geonics ProTEM system and the TerraTEM instrument from Monex GeoScope. Data were collected using these two systems in an interleaved fashion, with adjacent sites collected with different instruments. This approach resulted in higher productivity and permitted a comparison between the two instruments. Station locations are given in table 4.

All data were collected using a 100- by 100-m transmitter loop. The depth of investigation scales with the transmitter moment (transmitter current x transmitter loop area), with a rule-of-thumb placing the depth of investigation at 2 to 3 times the transmitter loop length, which here corresponds to 200 to 300 m. ProTEM data were collected in a central loop configuration, whereas TerraTEM data were collected in a coincident loop configuration. The use of different configurations stems from limitations in the design of each system and necessitates some differences in data processing. In theory, however, the resulting inverse resistivity models are directly comparable between the two systems.

Calibration of a TDEM system is essential to an accurate recovery of near-surface resistivity structure. Calibration, as referred to here, applies to a particular combination of data logger, transmitter, and receiver, and involves the characterization of system filters, measurement of the transmitted waveform, an assessment of system bias, and correction for

**Table 2.** Flight-line direction and spacing for the Oakland, Nebraska, study area.

| Traverse line azimuth | Tie line azimuth | Traverse line spacing (meters) | Tie line spacing (meters) | Traverse line distance (kilometers) | Tie line distance (kilometers) | Total (kilometers) |
|---|---|---|---|---|---|---|
| 127°/307° | 37°/217° | 270 | 14,000 | 371.0 | 14.0 | 385.0 |

timing and normalization errors. The ProTEM system used in this study was calibrated in 2009 at an established test site in Lyngby, Denmark (Geological Institute, 2002a, b). The TerraTEM system has not undergone rigorous calibration; as such the early-time data and hence the near-surface resistivity structure should be treated with caution.

**Table 4.** Time-domain electromagnetic station locations in the Oakland, Nebraska, study area.

[Coordinates relative to the North American Datum of 1983, Universal Transverse Mercator projection, Zone 14]

| Station | Easting (meters) | Northing (meters) | Instrument |
|---|---|---|---|
| 0 | 706234 | 4633836 | TerraTEM |
| 250 | 706113 | 4634060 | ProTEM |
| 500 | 705991 | 4634275 | TerraTEM |
| 750 | 705848 | 4634394 | ProTEM |
| 1000 | 705654 | 4634646 | TerraTEM |
| 1250 | 705517 | 4634847 | ProTEM |
| 1500 | 705424 | 4635045 | TerraTEM |
| 1750 | 705350 | 4635173 | ProTEM |
| 2000 | 705038 | 4635426 | TerraTEM |
| 2250 | 704879 | 4635587 | ProTEM |
| 2500 | 704979 | 4635815 | TerraTEM |
| 2750 | 704870 | 4636027 | ProTEM |
| 3000 | 704736 | 4636259 | TerraTEM |
| 3250 | 704608 | 4636469 | ProTEM |
| 3500 | 704484 | 4636682 | TerraTEM |
| 3750 | 704359 | 4636906 | ProTEM |
| 4000 | 704239 | 4637120 | TerraTEM |
| 4250 | 704132 | 4637338 | ProTEM |
| 4500 | 703987 | 4637679 | TerraTEM |
| 4750 | 703842 | 4637806 | ProTEM |
| 5000 | 703736 | 4637982 | TerraTEM |
| 5250 | 703646 | 4638248 | ProTEM |
| 5500 | 703500 | 4638429 | TerraTEM |
| 5750 | 703360 | 4638654 | ProTEM |
| 6000 | 703244 | 4638853 | TerraTEM |
| 6250 | 703120 | 4639074 | ProTEM |
| 6500 | 703066 | 4639390 | TerraTEM |
| 6750 | 702779 | 4639613 | ProTEM |
| 7000 | 702684 | 4639857 | TerraTEM |

For ProTEM stations, data were collected at a range of base frequencies (285, 75, 30, 7.5, and 3 Hz) using a combination of high- and low-frequency receivers together with low- and high-current transmitters. Average current was 2.5 and 8.5 ampere (A) for the low- and high-current transmitters, giving rise to an average transmitter moment of 25,000 A-m$^2$ and 85,000 A-m$^2$, respectively. All data were collected with air coil receivers with moments of 31.4 m$^2$ and 200 m$^2$ for high- and low-frequency coils, respectively. At each base frequency, readings were averaged between 4 and 15 seconds. A minimum of 20 such readings were taken to permit robust error calculation. Noise measurements were also taken at each station by acquiring data with the transmitter off. Such noise measurements are used during processing to determine the time at which actual data fall below the measured noise envelope.

For TerraTEM stations, data were collected using two different transmitters at three different current settings ranging from 0.5 to 25 A, giving rise to transmitter moments ranging from 5,000 A-m$^2$ to 250,000 A-m$^2$. In all cases, a coincident loop receiver with an area of 10,000 m$^2$ was employed. At each current setting, 10 to 15 readings were taken, each being the stack average of 250 transient decays. Noise measurements were also taken at each station.

## Audio-Magnetotelluric Method

The magnetotelluric (MT) method is a passive surface-geophysical technique that uses the Earth's natural electromagnetic fields to investigate the electrical resistivity structure of the subsurface. The MT method can be used to probe the crust from depths of tens of meters to tens of kilometers (Vozoff, 1991). Natural variations of the Earth's magnetic and electric field are recorded in two orthogonal, horizontal directions at each MT station. An optional third magnetometer measuring the vertical component of the magnetic field can help delineate some variations in resistivity related to different geologic materials and structures. The recorded time-series signals are used to derive apparent resistivities and phases. For a two-dimensional (2-D) Earth, the MT fields can be decoupled into transverse electric (TE) and transverse magnetic (TM) modes; 2-D modeling generally is done to fit both modes. When the geology satisfies the 2-D assumption, and the survey transect is oriented perpendicular to the geologic strike of interest, the MT data for the TE mode are for the electric field parallel to geologic strike (or perpendicular to the survey transect), and the data for the TM mode are for the electric field across strike (parallel to the survey transect). The MT method is well suited for studying complicated geological environments because the electric and magnetic relations are sensitive to vertical and horizontal variations in resistivity. An introduction to the MT method and references for a more advanced understanding are in Dobrin and Savit (1988) and Vozoff (1991).

High-frequency AMT signals are MT signals that range from approximately 10 Hz up to 100 kHz. Variations in ground electrical conductivity can be investigated from a few tens of meters to several hundreds of meters depth. The AMT technique images the shallow stratigraphy, alluvium-bedrock contacts, and bedrock structures associated with fracture zones. Traditionally the AMT technique was limited by a natural weakness of MT signal from around 1 kHz to 5 kHz. However, the natural MT fields in this band can be augmented

by providing additional signal power with a small battery-powered transmitter (the controlled source) that reduces the potential loss of resolution at what can be critical depths of investigation.

An AMT survey was performed along a profile at the Oakland study area (fig. 2) from April 20 to 24, 2009, using the Geometrics EH-4 STRATAGEM system (Geometrics, 2007). A total of 34 AMT soundings were recorded progressing from southeast to northwest (fig. 2, table 5). AMT data were nominally acquired every 250 m using the standard orthogonal E-H arrangement (fig. 3). STRATAGEM does not utilize a third magnetometer to measure the vertical component. The survey X-direction was set along the general northwest trend of the line (N.30°W.) and the Y-direction was set perpendicular to the line (N.60°E.). The general rule of thumb in magnetotelluric surveying is to use the right-hand rule (X goes into Y using your right hand) with Z-positive in the downward direction. Electric fields were measured using 15-m dipoles, and the magnetic fields used EMI BF-6 high-frequency magnetic induction coils (Geometrics, 2007). Time-series data are recorded and field-processed into cross-powers in real time by the STRATAGEM acquisition software. This allows for almost immediate quality control field checks of the acquired data. Each station required about 10 minutes for setup, 20 minutes for data acquisition, and about 10 minutes for demobilization and moving to the next station.

The collection of high-quality AMT data requires an awareness of the physical surroundings. Cultural features can affect the measured AMT responses, depending on where the station is sited. These features include fences, pipelines, communication lines, railways, and other manmade conductors. Buried power lines along roads resulted in some stations (for example, station 15 and 28) being relocated. Some poor-quality data were also recorded between stations 10 to 14. These data were impacted by large overhead power lines (stations 10, 11, and 12) and a sprinkler pivot (stations 12 and 13) that was not known to be powered until the TDEM and AMT data were acquired. The stations with more electromagnetic noise required more time because data acquisition had to be repeated several times so that more data could be stacked during processing. The effects of near-surface resistivity anomalies can cause what are known as static shifts in the data (Sternberg and others, 1988). Stations 30, 31, and 32 are repeats of stations 2, 3, and 4. On the first day of data acquisition, the STRATAGEM transmitter was not working properly. This problem was resolved by the second day and the stations repeated at the end of the survey. The survey and data acquisition ended when selected sites south of stations 33 and 34 could not be accessed due to active crop planting.

## Potential Field (Gravity and Magnetic) Methods

Gravity surveys, whether conducted on the ground or in the air, measure the gravity field of anomalous density variations within the Earth. Geologic interfaces having large density contrasts and large relief, such as the topographic surface and the crystalline basement surface, produce the largest gravity anomalies. Interfaces between sedimentary units generally produce small gravity anomalies. The subject of gravity exploration and application has been covered in much of the geophysical literature and information can be found in many text books including Dorbin and Savit (1988), Telford

**Table 5.** Audio-magnetotelluric station locations used in the Oakland, Nebraska, study area.

[Coordinates relative to the North American Datum of 1983, Universal Transverse Mercator projection, Zone 14. do, same as above]

| Station | Date | Easting (meters) | Northing (meters) |
|---|---|---|---|
| 1 | 20-Apr-09 | 706135 | 4633818 |
| 2 | do | 706004 | 4634026 |
| 3 | do | 705866 | 4634244 |
| 4 | do | 705817 | 4634494 |
| 5 | 21-Apr-09 | 705596 | 4634761 |
| 6 | do | 705414 | 4635065 |
| 7 | do | 705225 | 4635230 |
| 8 | do | 704975 | 4635482 |
| 9 | do | 704955 | 4635750 |
| 10 | do | 704956 | 4636007 |
| 11 | do | 704699 | 4636178 |
| 12 | do | 704551 | 4636356 |
| 13 | do | 704349 | 4636503 |
| 14 | 22-Apr-09 | 704198 | 4636700 |
| 15 | do | 704013 | 4636497 |
| 16 | do | 704021 | 4636782 |
| 17 | do | 703896 | 4636997 |
| 18 | do | 703893 | 4637251 |
| 19 | do | 703853 | 4637494 |
| 20 | do | 703755 | 4637743 |
| 21 | do | 703672 | 4637963 |
| 22 | do | 703607 | 4638201 |
| 23 | do | 703482 | 4638395 |
| 24 | do | 703358 | 4638645 |
| 25 | 23-Apr-09 | 703220 | 4638850 |
| 26 | do | 703103 | 4639073 |
| 27 | do | 703091 | 4639281 |
| 28 | do | 702688 | 4639454 |
| 29 | do | 702723 | 4639714 |
| 30 | do | 706009 | 4634031 |
| 31 | do | 705886 | 4634211 |
| 32 | do | 705802 | 4634504 |
| 33 | 24-Apr-09 | 703901 | 4636480 |
| 34 | do | 703901 | 4636267 |

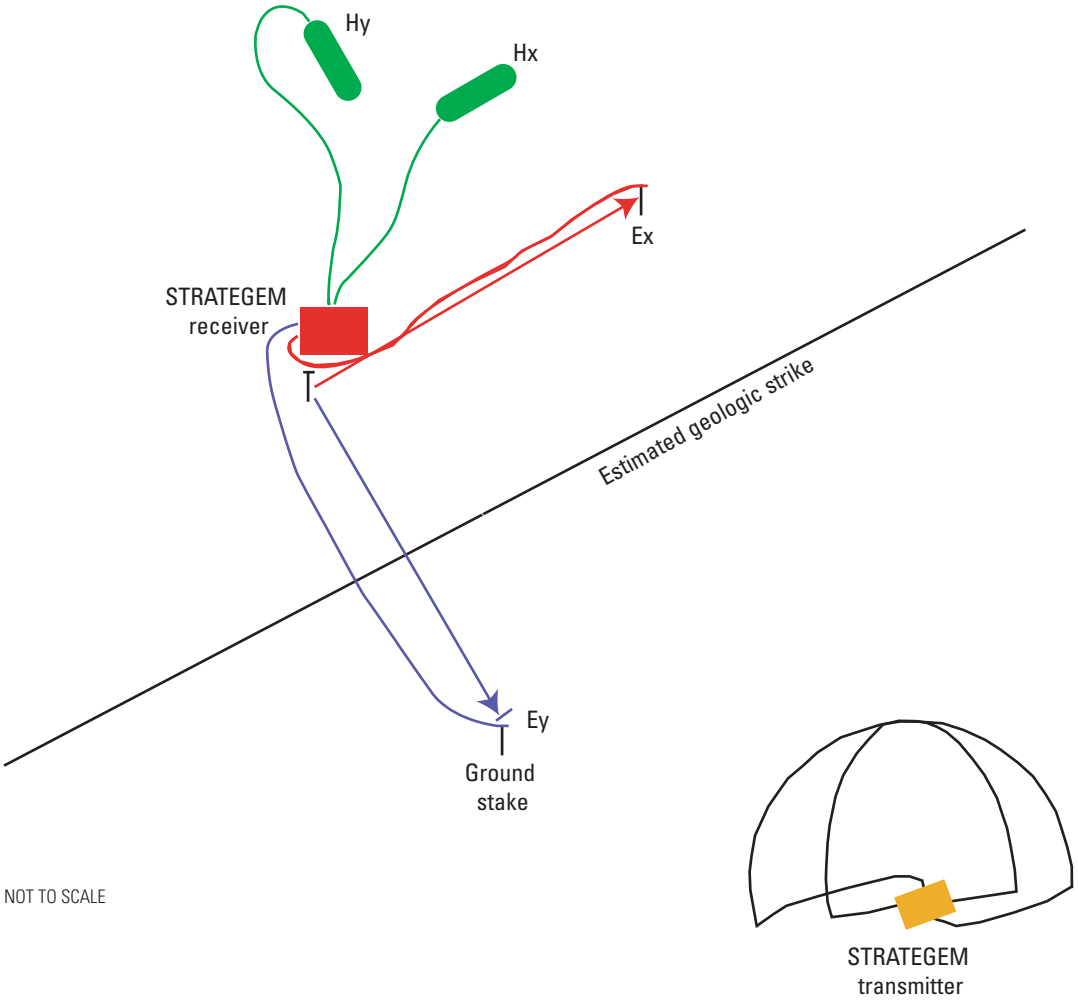


**Figure 3.** Schematic illustration of system layout for audio-magnetotelluric survey using STRATAGEM EH-4 system. Hx and Hy represent magnetic field receivers, and Ex and Ey represent the orthogonal ends of the dipoles used to measure the Earth's electric field. STRATAGEM transmitter usually was placed from 130 to 225 meters away from receiver station, depending on local near-surface geology.

and others (1990), Kearey and Brooks (1991), Blakely (1996), and Sharma (1997).

As discussed in a following section, the gravity anomaly produced from a sand and gravel paleochannel is small and a high-resolution meter is required to detect the feature. Ground-based gravity meters can resolve 1 to 5 microgallileo (μGal). Airborne gravimeters can achieve precisions of 0.5 to 1.0 milligallileo (mGal). Airborne gravity-gradiometer (AGG) systems have recently been applied to geological mapping (Dransfield and others, 2010; Murphy and Brewster, 2007). The precision achieved by the commercially available AGG systems is on the order of 3 eotvos (E) (Murphy, 2010). The E is the industry-accepted unit for AGG data (Lane and others, 2010). Currently all of the systems that are commercially available are within airborne platforms. Although these platforms are extremely good at mapping large areas, the cost of fielding an airborne system precluded its use in this study. For this study a high-precision ground-based gravity meter was selected.

Magnetic total field intensity changes are produced by variations in the magnetic mineral content of the geologic units and variations in the time varying diurnal field. The primary magnetic mineral found in the Earth is magnetite. Sedimentary rocks usually have low concentrations of magnetite in comparison to volcanic rocks or crystalline basement rocks. However near-surface sedimentary rocks can produce measurable magnetic anomalies if they contain sufficient magnetite and are folded, faulted, or truncated at an erosional surface. Ground or airborne magnetic surveys measure the total intensity of the Earth's magnetic field as the ground or airborne sensor follows survey lines either in the air or on the surface. The measured magnetic-field data are typically processed to remove time-varying diurnal fields and, if acquired from and airborne sensor, are corrected for noise from aircraft movements. The effects of Earth's primary magnetic field are removed to produce "magnetic anomaly data" that isolate subtle variations related to geology.

The subject of magnetic exploration and application has been covered in much of the geophysical literature, and information can be found in many text books including Dobrin and Savit (1988), Telford and others (1990), Kearey and Brooks (1991), Blakely (1996), and Sharma (1997). For this study an airborne magnetometer was used in conjunction with the HEM survey. Information on the magnetometer configuration and processing can be found in Smith and others (2008).

# Results of Investigation

For organizational purposes, this section discusses the results of each geophysical method separately.

## Helicopter Electromagnetic Results

The data from the Oakland study area were originally released as part of Smith and others (2008). This data release includes raw data, processed data, metadata, and the contractor's report. Apparent resistivities for each of the frequencies were provided by the HEM contractor and are included in Smith and others (2008). Cultural noise can have substantial impacts on EM data quality. Figure 4 shows the power-line noise channel in the HEM data; it reveals the extent of power lines in the survey area and how they are distributed along roadways.

As discussed in a following section, a 5- to 15-m thick layer with a conductivity of 0.1 to 0.2 S/m (5 to 10 ohm-m) is observed in the top 20 m of the surface. Table 6 gives calculated skin depths for the HEM frequencies for a medium with conductivity equal to 0.1 S/m (10 ohm-m). From this we can see that the thick layer of conductive (low resistivity) Earth encountered in the survey area severely limits the ability of the HEM method to image materials below it. In the worst case, only the lowest two frequencies can be expected to see through a 15-m layer of 0.2 S/m (5 ohm-m) Earth. This exercise illustrates that it is likely that the HEM signal will become too attenuated in the near-surface conductor to resolve geological layers below it. Nonetheless, HEM data were inversely modeled to better understand the distribution of subsurface resistivity and to more thoroughly evaluate the depth of investigation.

**Table 6.** Helicopter electromagnetic frequencies and theoretical skin depths for two different layer conductivities.

[Hz, hertz; σ, electrical conductivity; S/m, siemens per meter]

| Frequency (Hz) | Skin depth (meters) σ = 0.1 S/m | Skin depth (meters) σ = 0.2 S/m |
|---|---|---|
| 380 | 81.6 | 57.7 |
| 1,760 | 37.9 | 26.8 |
| 6,520 | 19.7 | 13.9 |
| 26,640 | 9.8 | 6.9 |
| 116,400 | 4.7 | 3.3 |

## Inversion of Electromagnetic Data

In-phase and quadrature responses at all five frequencies were inversely modeled using the code EM1DFM developed at the University of British Columbia Geophysical Inversion

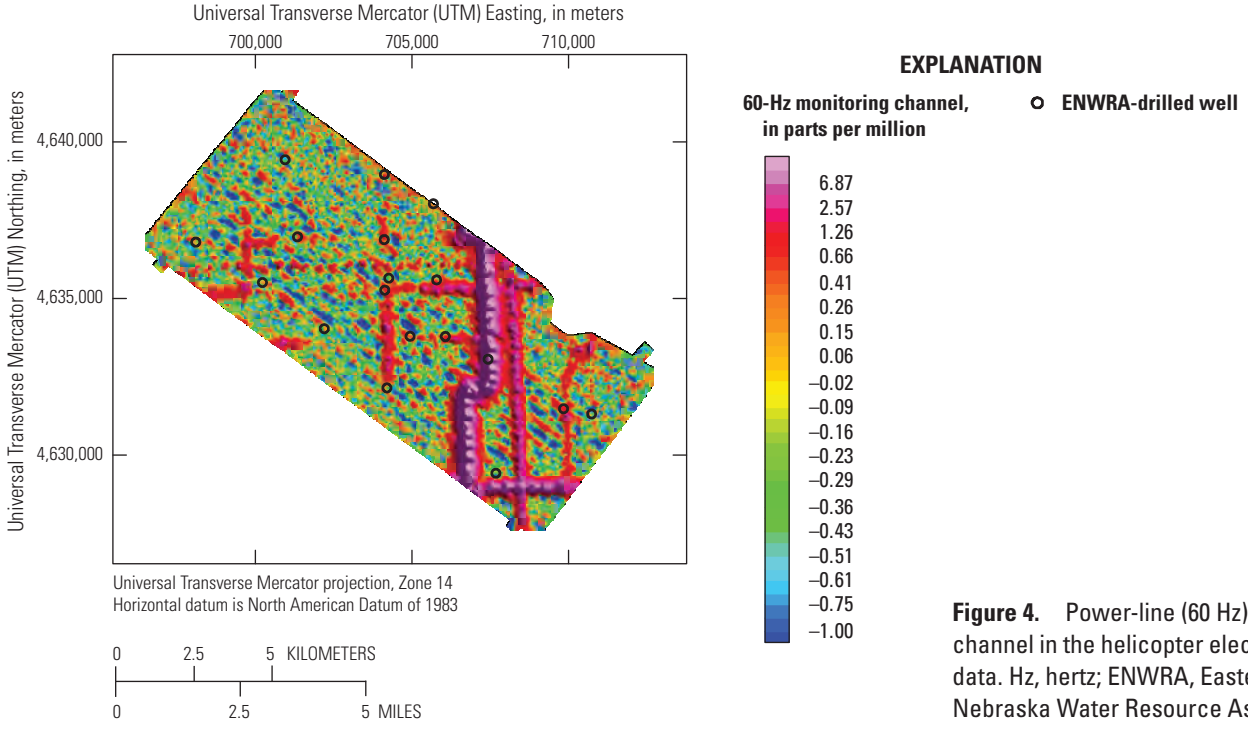


**Figure 4.** Power-line (60 Hz) noise channel in the helicopter electromagnetic data. Hz, hertz; ENWRA, Eastern Nebraska Water Resource Assessment.

Facility (Vancouver, B.C., Canada) to estimate the electrical resistivity structure of the subsurface. EM1DFM is a one-dimensional (1-D) inversion program that seeks the simplest resistivity model that adequately fits the observed in-phase and quadrature observations (Farquharson, 2000). The inverse problem is solved through an optimization scheme that iteratively seeks to minimize the model objective function, Φ, through the following simplified equation (Farquharson, 2000):

$$\Phi = \varphi_d - \beta\varphi_m$$

where $\varphi_d$ is the data misfit between the observed and calculated responses and $\varphi_m$ is a measure of the simplicity of the calculated model compared to a user-defined reference model. The trade-off parameter, β, ultimately weights the effects of the reference model and data misfit. Each sounding is interpreted without consideration to neighboring data and then profiled together to form a composite 2-D model. The theoretical background for EM1DFM is discussed in detail by Farquharson (2000).

EM1DFM requires several data and user-provided inputs. Data are compiled into an input file containing the frequencies, height of the sensor from the ground surface, in-phase and quadrature values, and estimates of the measurement noise. The user then creates a starting resistivity model that defines the initial resistivity estimates and layer distribution. Once these files are created, additional inversion parameters must be defined, including the type of inversion, reference model value, weighting factors, model norm components, tolerance, and the number of iterations.

All data were inverted for resistivity using the fixed trade-off parameter algorithm with a single-value reference model. The β value, model norm components, tolerance, and the number of iterations were identical for the entire study area. A 25-layer starting resistivity model was used to define the initial model domain. A site-specific single resistivity value was chosen based on the most common background resistivity values observed in the differential resistivity sections for each study area. Model settings are provided in table 7.

**Table 7.** Final parameters used during inverse modeling of helicopter electromagnetic data.

[Data were inverted using the fixed trade-off parameter algorithm with a 25-layer, 120-meter-thick starting conductivity model. Model parameters defined in Farquarson (2000). acs, weight for the layer in the smallest component of the conductivity portion of the model norm; acz, weight for the difference between layers in the flattest component of the conductivity component of the model norm]

| Starting resistivity model (ohm-meters) | Reference resistivity model (ohm-meters) | Fixed trade-off parameter (beta) | Maximum iterations | Tolerance | Model norm components (acs, acz) |
|---|---|---|---|---|---|
| 10 | 33, 10 | 1,000 | 15 | 0.01 | 0.01, 1 |

## Selection of the Trade-Off Parameter

Choosing an appropriate trade-off parameter, β, is critical to finding a geologically realistic final solution to the inverse problem (Farquharson and Oldenburg, 2004; Lipinski, 2007). For the HEM data, the fixed trade-off parameter algorithm was used, in which β is a user-defined value that remains constant for all soundings. Through a trial-and-error process, a β value is sought that results in calculated responses that honor the observed data within a reasonable range of the noise while not introducing unnecessarily complex resistivity structures.

Logarithmic values of β between 1 and 100,000 were attempted. Inversion results for selected lines from each study area were then manually examined for over-fitting to both the reference model (resulting in oversimplified models) and the measurement noise (resulting in unreasonably complex models). Results were compared to co-located lithologic logs and TDEM soundings to evaluate the positioning of electrical layers. Differential resistivity sections (Smith and others, 2008) from the HEM data were also used to evaluate the model complexity. Based on these comparisons, a β value of 1,000 was determined to be appropriate.

Figure 5 illustrates the effect of changing β values on the model results from a single flight line from the Oakland study area, line 10010. All other model settings were held constant, and a reference model of 10 ohm-m was used. As the β value is increased from 10 to 10,000, the appearance of noise inherited from the observed data is reduced, and the model appears more consistently like the single-value reference model. Some features, such as the high-resistivity layer centered near Easting 708,100, remain present regardless of the β value used; this indicates that this layer is relatively robust, and even with a heavily weighted reference model, the observed data demand its presence. The moderate-resistivity (50 ohm-m) layer throughout the remainder of the profile is less consistent between β values. This layer appears most strongly in the scenario with the β value of 10 (fig. 5*C*). Because this layer is more resistive than the reference model and more clearly expressed as the observed data are more strongly weighted, it is interpreted as a weakly resolved geologic contrast. Limited borehole data exist for the Oakland study area, and although throughout the site a glacial till layer is inconsistently described near the top of this electrical layer, the geologic source of this feature is uncertain.

## Sensitivity-Based Approach to Exploration Depth Estimation

Exploration depth is dependent on both the transmitted frequency and the resistivity of subsurface, as approximated by skin depth, $z_e$ (Telford and others, 1990, p. 309):

$$z_e = 500\,(\rho/f)^{1/2}$$

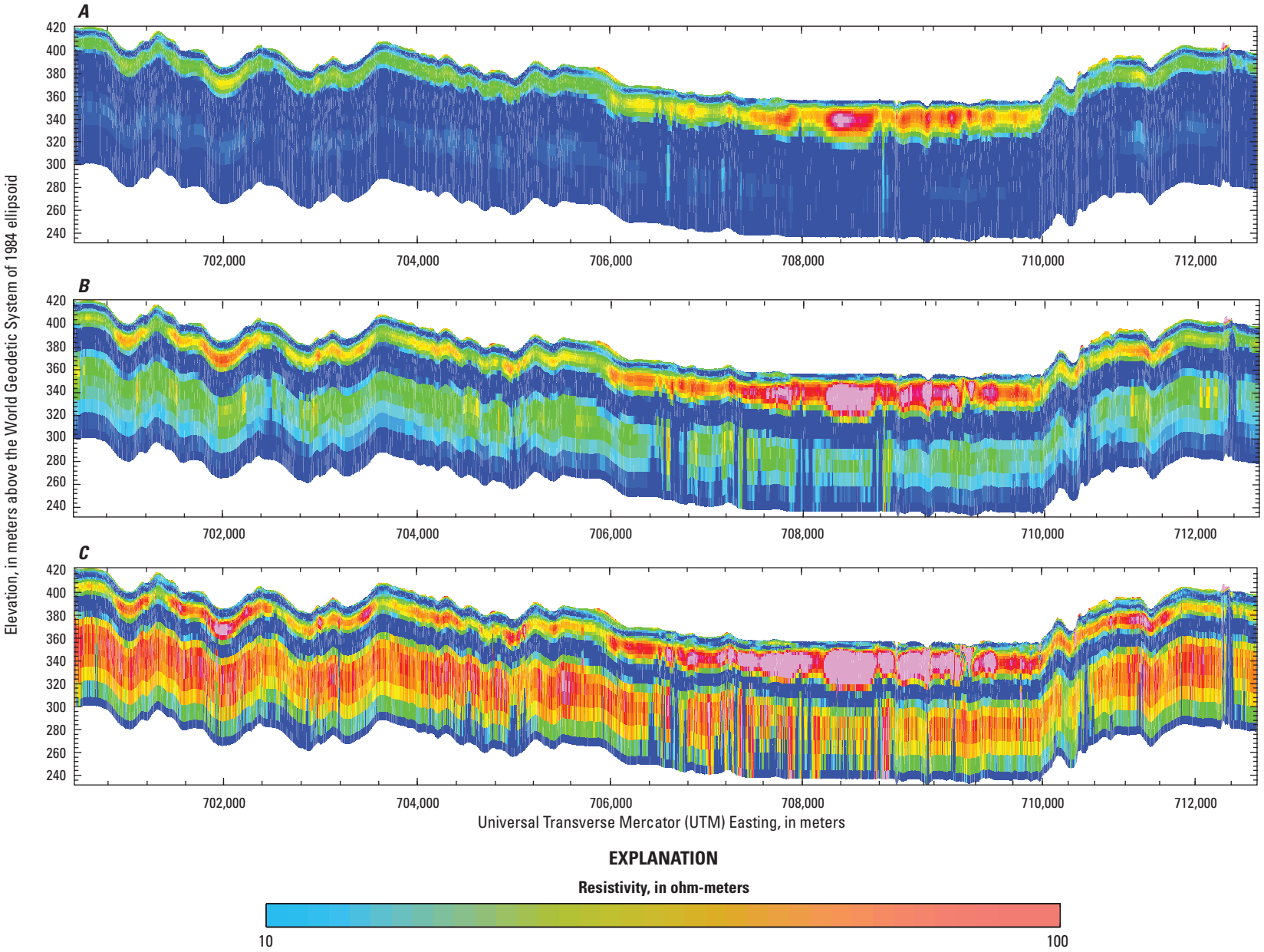


**Figure 5.** Profiles of inverted resistivity models for helicopter electromagnetic flight line 10010 from the Oakland, Nebraska, study area demonstrating the impact of different trade-off (beta) parameters on the inversion result. Beta values of *A*, 10,000, *B*, 1,000, and *C*, 100 are shown.

where ρ is the subsurface resistivity (ohm-m), and *f* is the EM frequency (Hz). As the transmitted frequency increases, the signal attenuates more quickly in the near surface resulting in a decrease in exploration depth. However, skin depth also shows that decreasing subsurface resistivity can also substantially reduce exploration depth. Therefore, as resistivity structure changes throughout the study area, the sensitivity with depth also changes. Here we present a differencing approach that allows us to evaluate the sensitivity of the inversion process to the observed data. This facilitates the removal of regions where the user-defined model settings are controlling the final calculated resistivity.

To better evaluate the sensitivity-limited exploration depth of the final inversion model, all data were inverted using two different reference models (table 7). Where the final model is relatively insensitive to the observed data, the reference model dominates the final model resistivity. If there is greater than 40 percent difference in model resistivity between the two inversions at any given model cell location, the model cell is removed. In effect, this technique leaves the robust data unaltered and removes low-sensitivity areas. This provides the ability to determine a more realistic exploration depth, and data below the region where the majority of the signal has been attenuated do not show and are thus not interpreted.

This differencing approach is illustrated in figure 6 for a single line from the Oakland study area, line 10010. Figures 6*A* and 6*B* show that, though the majority of the resistivity structure remained nearly identical, model values in the lower 70 m of the profiles were inherited from the reference model, 33 ohm-m and 10 ohm-m, respectively. The resistivity value of each model cell location was compared between the profiles, and where the difference exceeded 40 percent, the model cell was removed from the final profile (fig. 6*C*).

## Interpretation

The differencing procedure allows a thorough examination of the HEM system's ability to define the paleochannel observed in the lithologic descriptions from the ENWRA drilled wells. Figure 7 shows the inverted HEM section of the northwestern portion of flight line 10010. Lithologic records from the two wells closest to the line, 32-EN-07 (about 65 m northeast) and 30-EN-07 (about 250 m northeast) illustrate that the shale layer defining the bottom of the paleochannel is at least 10 m deeper than the HEM system was able to resolve using this analysis approach.

Examination of all inverted flight lines shows some basic trends in resistivity (figs. 7–9). In general, a thin, low-resistivity layer overlies a thicker, moderate- to high-resistivity layer that is underlain by a thicker, low-resistivity layer. The bottom of the inverted sections hints at a higher resistivity layer at depth that may represent the Dakota Formation, but this layer is poorly resolved due to the thickness and resistivity of the overlying material (figs. 7 and 8). The most prominent feature seen in the inverted data is the high-resistivity material in the immediate vicinity of Logan Creek (fig. 9). The Logan Creek valley sediments are characterized by silt and clay units that overlie sand and gravel deposits. Hole 29-EN-07 was drilled in an area where the HEM survey indicated highly resistive material at depths of about 6.0 to 27.4 m. Lithologic samples and down-hole geophysical logs confirmed the presence of sand and gravel deposits from 5.5 m to 26.5 m overlying a shale bedrock. Resistive units identified in the HEM survey 4.82 km north of this site were confirmed from analysis of a CSD test hole drilled in 1950.

## Time-Domain Electromagnetic Results

TDEM soundings were collected in a profile across the suspected paleochannel in the northwestern portion of the Oakland study area. Data quality is highly variable and primarily reflects proximity to cultural noise. Inductive coupling, due to metallic subsurface conductors, was identified within the central segment of the profile in close proximity to a series of underground natural gas transmission lines. At these locations data quality is compromised at late times (oscillatory behavior in the dB/dt decay curves), but removal of the late-time data results in interpretable data. Stations strongly affected by inductive coupling to the pipeline include 2000, 2250, 2500, and 2750 (fig. 2). More problematic is galvanic coupling, commonly associated with power lines (fig. 4), which results in a smooth, yet artificial, enhancement of the dB/dt decay curve. Galvanic-coupled data can only be identified by jointly examining a number of nearby stations and cannot be effectively corrected. Stations 0, 1500, 1750, 4500, 6750, and 7000 all show evidence of galvanic coupling (fig. 2) and have therefore been excluded from further analysis. Finally, stations 3000 and 3750 have decay curves that deviate significantly from neighboring stations; this behavior is attributed to cultural noise of unknown origin, and these sites have been excluded. In total, 21 of the 29 measured stations were deemed acceptable for further processing and inversion.

## Analysis of Time-Domain Electromagnetic Data

Data analysis for all soundings consisted of data format conversion, statistical analysis and averaging, forward modeling, data inversion, and model assessment. Data were processed and inverted using the SiTEM data processing and Single-site Electromagnetics Data Inversion (SEMDI) software packages (Auken and Nebel, 2001). The SEMDI inversion permits full waveform specification, the modeling of system filters, and the incorporation of data errors. Furthermore, it provides error bounds on inverted layer thicknesses and resistivities. Data were inverted for two end-member model classes—minimum-layer models and 20-layer smooth inverse models. The former class of models seeks to fit the measured data with as few distinct layers as possible, whereas the latter seeks to fit the data with a large number of thin layers under the constraint that the resistivity varies slowly between adjacent layers. Minimum-layer models may be more

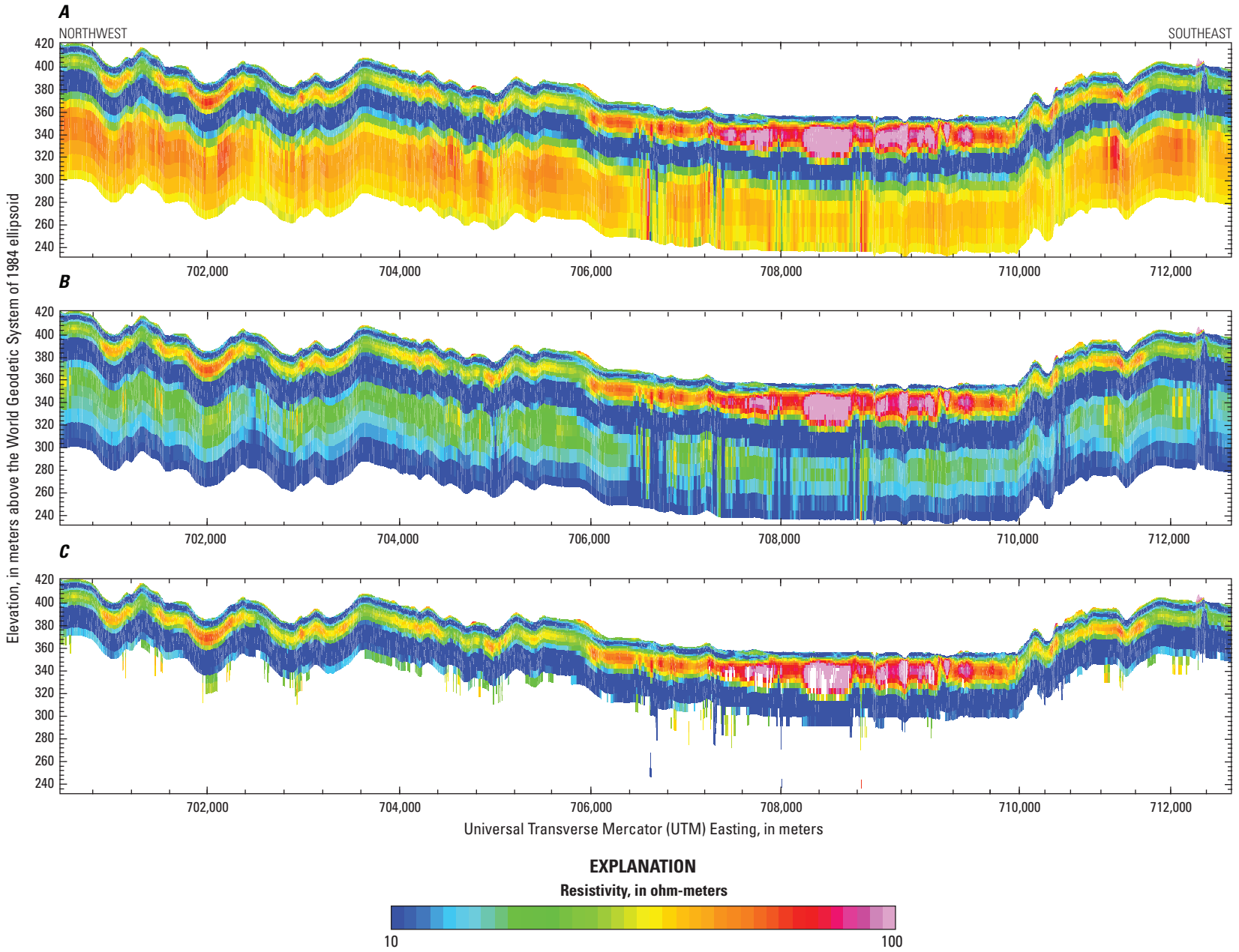


**Figure 6.** Profiles of inverted resistivity models for helicopter electromagnetic flight line 10010 from the Oakland, Nebraska, study area demonstrating the differencing approach used to evaluate model sensitivity and determination of exploration depth. The inverted resistivity model using *A*, a 33 ohm-meter reference model was compared to the model using *B*, a 10 ohm-meter reference model. The areas that were highly sensitive to the reference model setting were removed, resulting in *C*, the final inversion model used for interpretation. A trade-off parameter value of 1,000 was used for all three inversions.

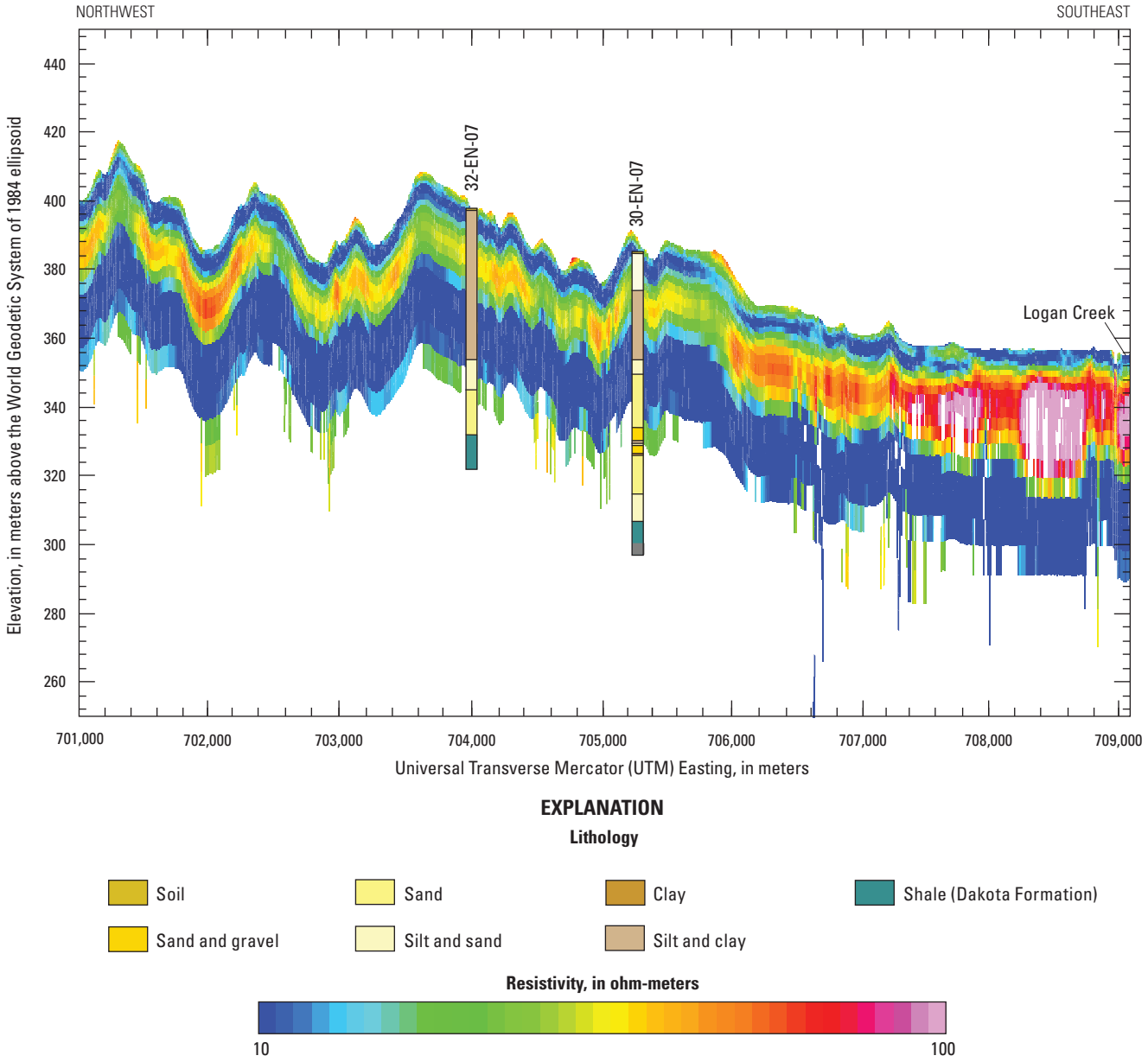


**Figure 7.** Inverted resistivity section of part of helicopter electromagnetic flight line 10010 from the Oakland, Nebraska, study area. Lithologic data from nearby Eastern Nebraska Water Resource Assessment drilled wells are shown for comparison.

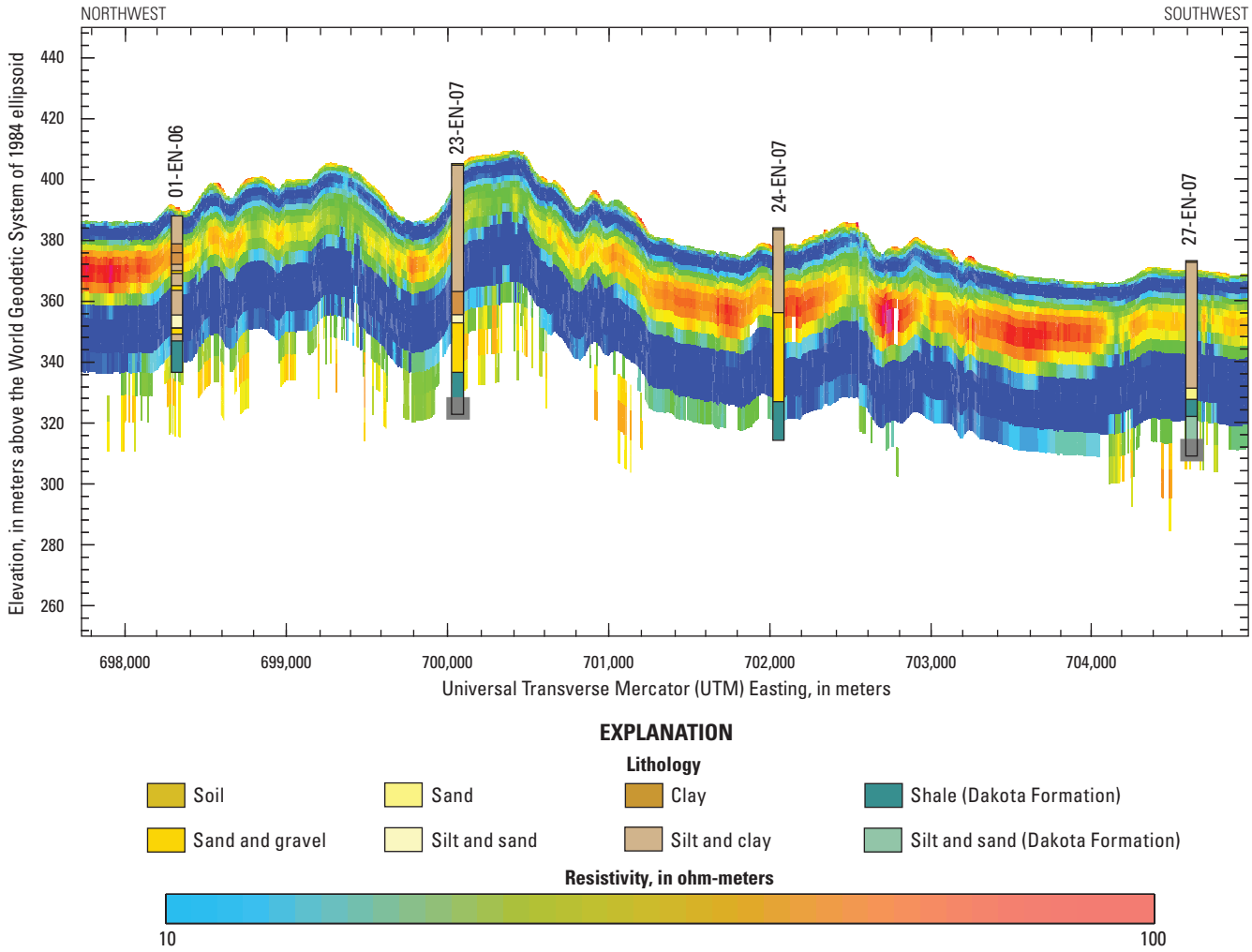


**Figure 8.** Inverted resistivity section of part of helicopter electromagnetic flight line 10200 from the Oakland, Nebraska, study area. Lithologic data from Eastern Nebraska Water Resource Assessment drilled wells are shown for comparison.

appropriate in settings where sharp variations in resistivity are expected, whereas smooth inverse models may be more realistic when gradational changes are expected. Independent knowledge from geologic mapping, borehole lithology, and geophysical borehole logs are typically used to assess which of the above model classes may be more appropriate in interpreting subsurface structure.

The modeling and inversion of TDEM data are commonly 1-D. This assumption is reasonable given the nature of the regional geology (laterally expansive glacial deposits) and the limited depth of investigation (100 to 300 m). Furthermore, lithologic logs from surrounding drill holes show correlation across the study area. Finally, the layered-earth assumption appears validated by the final 1-D inverse models, which, at least in the upper 100 m, generally show smooth variation in interface depths from station to station.

All geophysical inverse problems exhibit a degree of non-uniqueness, the TDEM method included. The non-uniqueness stems from both inherent resolution limitations and incomplete and inexact data. Thus, for any measured dataset, a range of models can typically be found that adequately fit the data. For most electrical methods, equivalence exists between models with equal conductance or integrated conductivity. Thus, for example, a model with a 10 ohm-m, 50-m-thick layer produces nearly identical measured data as a 25-m-thick layer of 20 ohm-m resistivity. Additionally, the TDEM method has difficulty resolving resistive layers due to the low current densities induced within them as compared to conductive layers.

Looking to the minimum-layer models, the data generally support a four-layer resistivity structure with a near-surface conductive layer of 12 ± 1 ohm-m (fig. 10*A*). The thickness of this layer varies across the profile (50 ± 20 m) but is thickest at the north and south ends of the profile (approximately 90 m) and thinnest in the central portion of the profile (approximately 25 m). A second, more resistive layer appears segmented along profile, with a northern section (sites 4500–6500) characterized by a resistivity of 20 ± 3 ohm-m, a central section (sites 3000–4250) by a resistivity of 34.7 ± 10.4 ohm-m, and a southern section (sites 250–1250) by a resistivity of

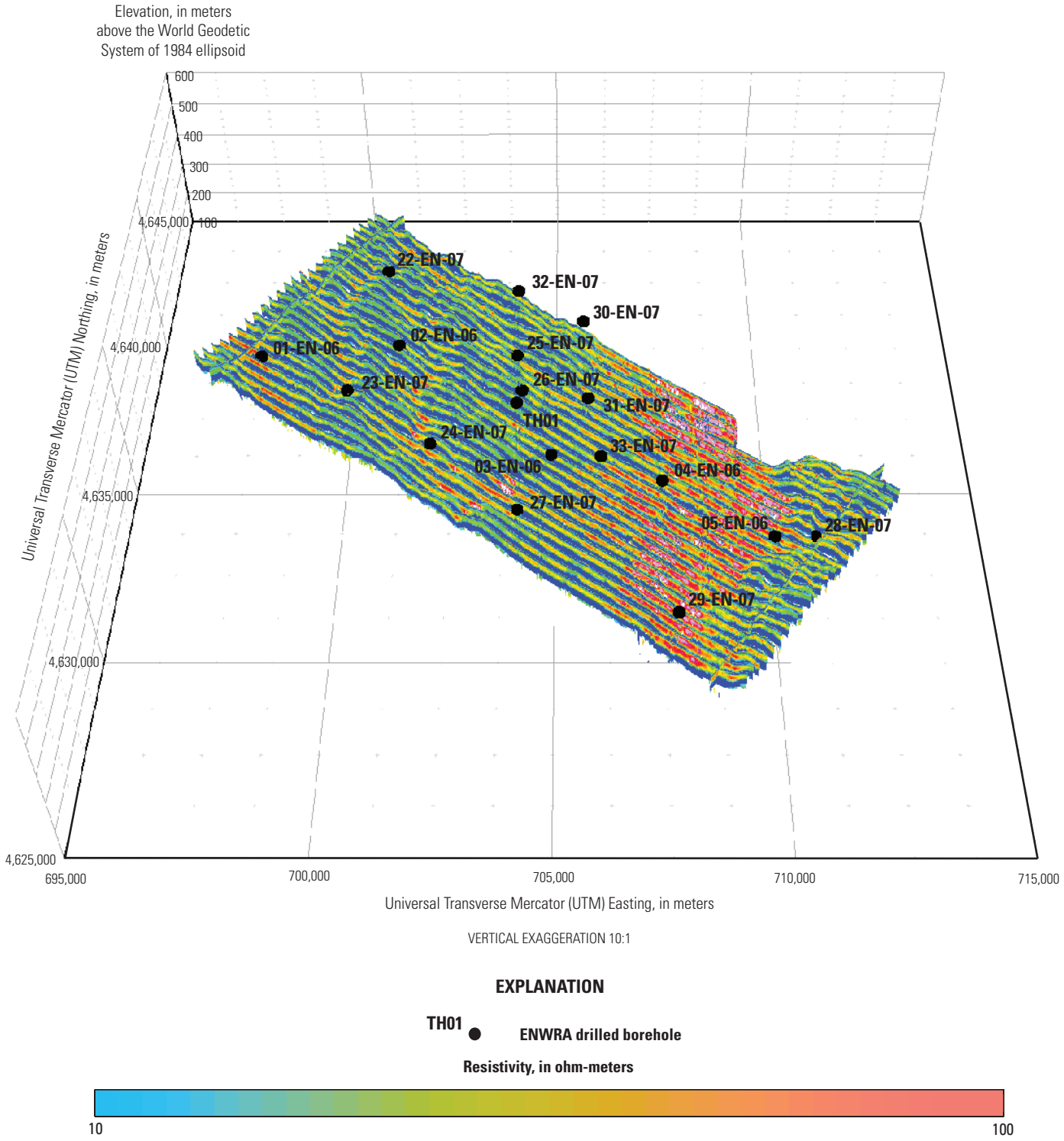


**Figure 9.** Three-dimensional map of the Oakland, Nebraska, study area showing inverted helicopter electromagnetic resistivity sections and borehole locations. ENWRA, Eastern Nebraska Water Resource Assessment.

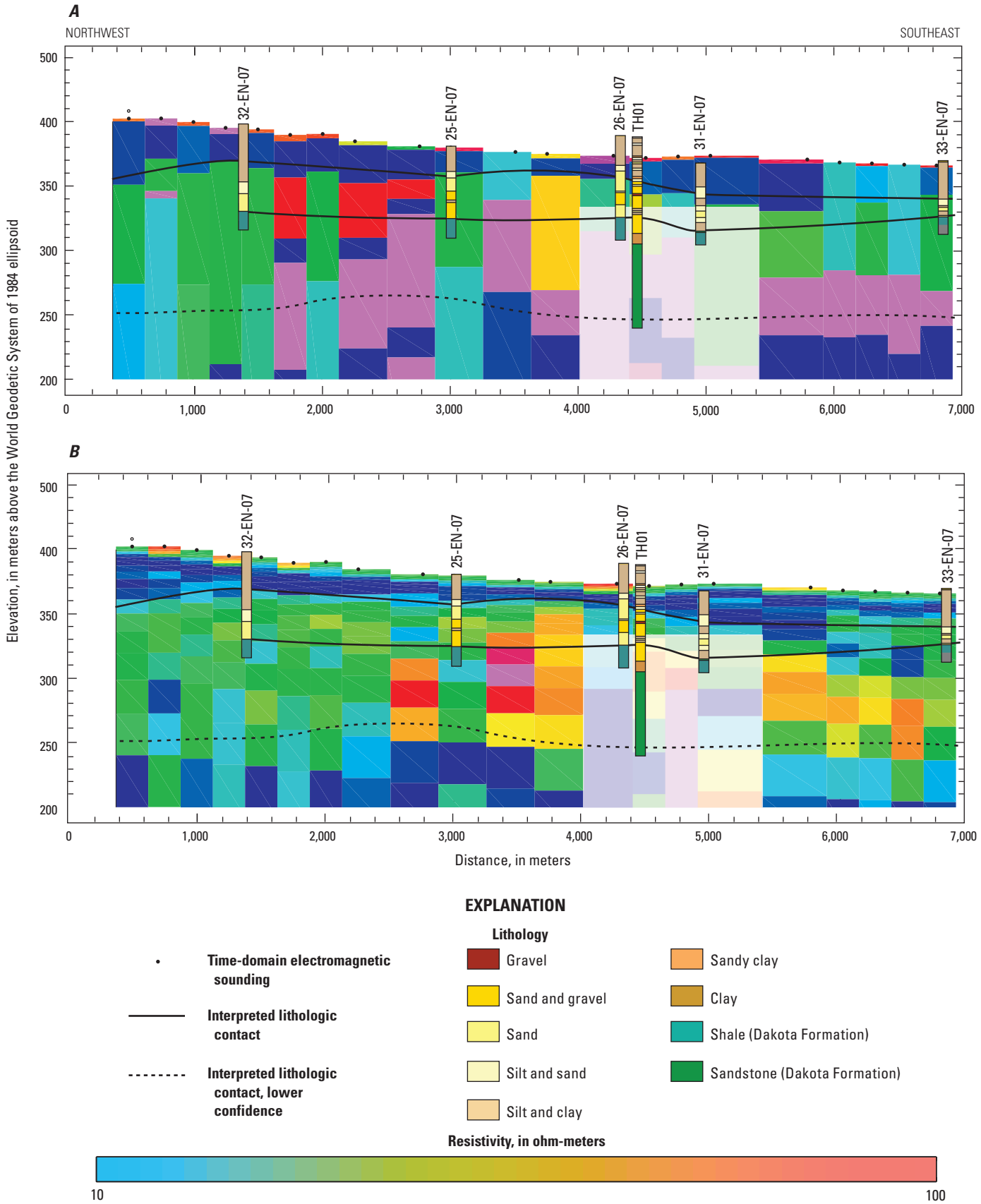


**Figure 10.** Stitched sections showing one-dimensional time-domain electromagnetic inversion results for *A*, minimum-layer and *B*, smooth models from the Oakland, Nebraska, study area. Lithologic data from Eastern Nebraska Water Resource Assessment test holes are projected onto the line, and lithologic contacts are interpreted based on both lithologic and inversion results.

36 ± 9 ohm-m. The structural connection between the northern and central sections cannot be unambiguously determined by the TDEM data. This is due to the degradation in data quality at stations 2000–2750 attributed to cathodic protection on natural gas pipelines running beneath these sites. This resistive layer shows some thickness variation, thinning from approximately 100 m in the north to approximately 80 m in the south. Beneath the resistive layer is a highly conductive layer with an average resistivity of 9 ± 3 ohm-m. The high-conductivity zone appears thickest beneath the thick resistive packages and thins out considerably where these resistive zones similarly thin. Beneath all the above structure is a resistive zone at depths ranging from 100 to 300 m. The resistivity of this deepest structure is largely unconstrained.

## Interpretation

Stitched 1-D model sections are shown in figures 10*A* and 10*B* for the minimum-layer and smooth inverse models, respectively. Both model sections suggest continuous layering in the near surface. Using the minimum-layer model as a guide, a thin veneer (3 to 4 m) of moderately resistive material (60 ± 30 ohm-m) overlies a highly conductive layer (11 ± 1 ohm-m) across the entire profile. This conductive layer is approximately 30 m thick on the north and south ends of the profile, thinning to less than 15 m beneath the central profile. The high conductivity likely reflects clay and silt within the thick glacial till, whereas the more resistive capping layer may reflect a rather thin unsaturated zone.

Beneath the conductive glacial till, a layer of variable resistivity is imaged; beneath the north and south ends, this layer has a resistivity of 15–20 ohm-m, but increases to 60–70 ohm-m beneath the central profile. Both smooth and minimum-layer model sections suggest the resistive zone pinches out to the north. However to the south, the minimum-layer model sections show a gradual thinning, whereas the smooth model sections suggest it pinches out. This resistive zone to first order agrees with the sand and gravel region identified from borehole lithology. It is unclear if this represents changes in grain size and sorting within a continuous depositional layer or the emplacement of sand and gravel within a paleochannel. Beneath this layer, at approximately 130 m deep, is a relatively flat conductive layer (8–15 ohm-m) that extends across the profile. The conductance of this layer, combined with its depth, makes it difficult to resolve structure much below 200-m depth. There is some indication of an increase in resistivity at greater depth (not shown), but this is poorly constrained.

Comparison of the model section to test-hole lithologic data shows a clear correspondence with the transition from silt and clay (glacial till) to sand and gravel. The strongest mismatch occurs between the model and test hole 32-EN-07 and likely reflects its distance from the profile (about 1 km, fig. 2). Interpolation of the full set of test-hole lithologic data indicates a thickening of the glacial till northeast of the profile, consistent with the thicker till section present in test hole 32-EN-07. Below the glacial till, correspondence begins to diverge between the model and the lithologic logs. The model section favors a thick layer of variable resistivity atop a highly conductive layer at approximately 130-m depth. In contrast, the lithologic logs indicate a layer of sand and gravel, as much as 50 m thick, atop a clay-shale layer at 70- to 80-m depth that was not penetrated by any of the test holes. It is noted, however, that both the model section and the lithologic logs suggest that the resistive sand and gravel are thickest beneath the central profile and thin to the north and south.

The mismatches between the TDEM models and the test-hole data are due to several factors. Layer conductance and the elevation of the top of a strong conductor are the two best resolved parameters using electrical and EM methods. We are confident that the top of the conductor is about 130 m deep. Between the base of the glacial till and this layer there is roughly 100 m of material, which according to the TDEM sections is no less than 20 ohm-m (0.05 S/m); this corresponds to a conductance of 5 siemens (S). The lithologic logs indicate at most 50 m of sand-gravel with 50 ohm-m (0.02 S/m) resistivity, or a conductance of 1 S. The underlying clay-shale layer is approximately 5 to 10 m thick; however, this estimate is based on only one test hole (TH01) that penetrated through to sandstone. Based on borehole log resistivities of 10–20 ohm-m (0.05–0.01 S/m), this clay zone contributes another 0.5 S. Thus to the depth that the borehole logs sample, 1.5 S can be accounted for. This suggests several things. First, there are more conductive layers below the depth of the clay shale encountered at 70 to 80 m at the bottom of the test holes. Second, the TDEM models do not have the resolution to differentiate the thin clay-shale from the overlying sand-gravel package. Instead, a bulk resistivity that averages both of these units as well as a deeper source of conductivity was recovered. The lack of resolution can be attributed both to the thickness-to-depth ratio of the target and the overlying thick conductive till, which attenuates the induced subsurface currents. Thus, though the configuration of the sand-gravel package cannot be well constrained, the TDEM models do recover along-profile variations in sub-till resistivity that correlate with the location of the sand-gravel as identified in lithologic logs. Ground TDEM surveys can thus provide a means for identifying regions of sand and gravel beneath thick conductive till.

# Audio-Magnetotelluric Results

AMT soundings were collected in a profile across the suspected paleochannel in the northwestern portion of the Oakland study area in a line similar to that of the TDEM data. The recorded AMT time-series data were transformed to the frequency domain and processed to determine a 2-D apparent resistivity and phase tensor at each station. Time-series datasets were selected for optimal signal-to-noise characteristics prior to the cross-power calculations. Noisy data in the time-series, spectral, and resistivity data were culled out. Cross-power and MT impedance data files were created with the STRATAGEM data acquisition program IMAGEM. These

files are used as input to the 2-D inversion modeling program. Since the STRATAGEM is a single-station MT sounding system, remote reference processing, as discussed in Gamble and others (1979), and then more advanced multistation processing (Egbert, 1997) could not be utilized. Several of the noisier sites would have clearly benefited by the use of remote reference stations.

During the 2-D analysis and interpretation process, each station was rotated to a fixed angle (60°) determined by the perpendicular direction to the given nominal profile orientation of N.30°W. Rotation of the impedance tensor allows for decoupling into the TE and TM modes.

A measure of the dimensionality for MT data is provided by the impedance skew of the impedance tensor (Vozoff, 1972). If the effective measured resistivity response to the geology beneath an AMT station is truly 1- or 2-D, then the skew will be zero. Instrument and environmental sources of electrical noise can cause nonzero skew values. Skew values typically are small (about 0.1) for relatively low noise recordings. Higher skews (above 0.2) are an indication of either the resistivity response to 3-D geology or higher levels of noise. Manmade electrical noise, such as power lines, power generators, and moving vehicles and trains, can have a negative effect on AMT data quality. All of these local disturbances can produce incoherent noise that mainly affects frequencies above 1 Hz. Other manmade electrical noise, such as direct-current electric trains and active cathodic protection of pipelines, produces coherent electromagnetic signals that mainly affect frequencies below 1 Hz.

## Analysis of Audio-Magnetotelluric Data

A 2-D inverse and forward modeling analysis of the Oakland AMT data was performed. Wannamaker (1983) found that although some AMT responses are fundamentally 3-D in nature, for elongated structures, 2-D modeling could be used to construct reasonable estimates of the resistivity cross sections along each profile. Wannamaker and others (1984) demonstrated that approximating 3-D structure beneath a centrally located profile with 2-D modeling is best achieved when fitting the TM curve, even at the expense of a poor fit of the TE curve. However, because TM data are relatively insensitive to the depth extent of a subsurface body (Eberhart-Phillips and others, 1995), the depths to the base of the bodies in the model are not well constrained. Hence, mixed mode analysis (modeling the TM/TE mode) may help clarify the modeling results.

Two-dimensional resistivity models were constructed for the 7-km-long profile. Not all soundings were included in the inversion analysis, because of the separation distance between stations that is required by the inversion program. The projection of stations 15, 33, and 34 onto the survey transect puts stations 15 and 33 almost directly on top of each other and right next to station 14 (fig. 2). Station 34 becomes too close to station 13. Station 14 was selected for use in the inversion because it was closest to the survey transect. Since station 13 was somewhat contaminated by the powered sprinkler pivot, it was not used in the inversion, and station 34 was used in its place.

The 2-D inversions of the AMT data were conducted using the computer program RLM2DI (Mackie and others, 1997; and Rodi and Mackie, 2001) from within GEOTOOLS (Geotools, 1998), a shell program specifically designed to process and interpret MT and AMT data. This was followed by the application of the 2-D forward modeling algorithm program, PW2D, developed by Wannamaker and others (1987). The results of the RLM2DI 2-D inversion were used as the initial input model for the forward modeling, PW2D, where a sensitivity analysis was performed on the conductive structures derived from the inversion results.

RLM2DI uses a finite-difference network analog to the Maxwell's equations governing the magnetotelluric method to calculate the forward solution and a nonlinear conjugate-gradient-optimization approach that is applied directly to the minimization of the objective function for the inverse problem. PW2D is a stable finite-element algorithm that simulates transverse electric and magnetic fields using a linear basis across each finite element. The inversion algorithm, RLM2DI, was usually allowed to batch run 25 iterations in order to reduce to a reasonable value the root-mean-square error between the field data and the numerical model. The number of iterations of forward modeling (PW2D) necessary depended on how complex the profile inversion results were from RLM2DI.

The RLM2DI inversion model for the Oakland AMT data used 92 horizontal cells and 59 vertical cells. The number of horizontal and vertical nodes necessary for the iterative forward modeling (PW2D) algorithm to accurately model the subsurface resistivity distribution in the Oakland area was greater than the number of cells required by the inversion algorithm. This is a function of some fundamental differences between how finite-difference and finite-element algorithms handle the numerical boundary conditions and, subsequently, how the electric and magnetic fields were calculated across the mesh. The forward model used 134 horizontal and 62 vertical cells.

The edges of the forward model were extended horizontally and vertically to minimize edge effects. The resolution of the resistivity boundaries used for each model is somewhat subjective. If different resistivities were used, then boundary positions and layer depths would have to be adjusted to achieve similar fits to the observed data. The extreme case would be to use a model with a "continuous" resistivity gradient from low to high resistivities. The resolution of the resistivity boundaries is also, in part, a function of the model grid-mesh design. The models' depths were assigned relative to the Earth's surface. Nine additional vertical nodes are usually added to model the overlying air layer.

## Interpretation

The results for the TM-mode inverse modeling are presented in figure 11*A*. This allows for a better spatial perspective on the relations between the different resistivity distributions. From the ground surface, there is a 5–10 ohm-m layer

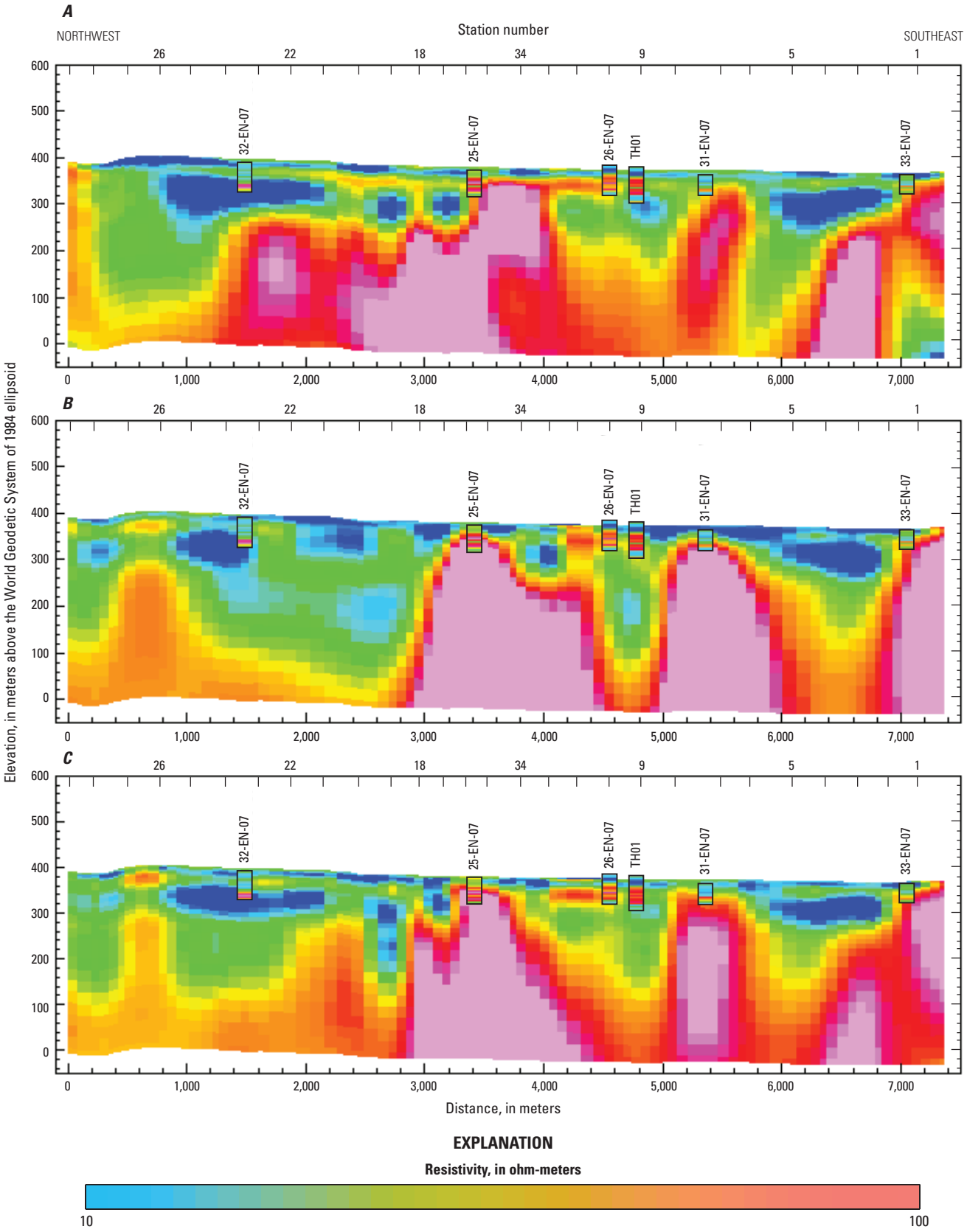


**Figure 11.** Two-dimensional inverse models of audio-magnetotelluric data for the *A*, transverse magnetic (TM), *B*, transverse electric (TE), and *C*, mixed TM/TE modes from the Oakland, Nebraska, study area. Short-normal (16 inch) borehole resistivity logs are projected onto the line. Inverse models and borehole logs are displayed with the same resistivity color scale.

that is 5–15 m thick extending along the entire transect. On the northwest end of the line, between stations 25 to 28, this conductive zone is thickest. It begins at the ground surface and extends down to about 25-m depth. Elsewhere the depth to the top of this conductive zone is about 10 m.

There is an electrically resistive zone (50–200 ohm-m) in the center of the profile between 25-m and 60-m depth. This zone begins just northwest of station 10 and ends just southeast of station 16. This zone may in fact be two different materials as it is more resistive on the northwest side (stations 34 and 14) and less resistive on the southeast side (stations 11 and 12). The zone under stations 34 and 14 extends deeper than that under stations 11 and 12. At around 130-m depth, the resistive zone under stations 34 and 14 begins to spread out, and then below 150-m depth, the zone extends laterally from beneath station 24 to station 11.

The resistive zone beneath stations 18, 19, 20, and 21 between 25-m and 60-m depth may be the same material as in the center of the profile (figs. 2 and 11). Similarly, a smaller resistive zone is located beneath stations 6 and 7 beginning at 40-m depth and extends to greater depths with a slight northwesterly dip. A third resistive zone is located beneath stations 1, 30, 31, and 32 at depth with resistivities ranging from 50–200 ohm-m.

There are also two conductive zones of interest. One is beneath stations 22, 23, 24, 25, and 26 and the other beneath stations 30, 31, 32, and 5 (figs. 2 and 11). The northwest conductive zone is between around 50-m and 100-m depth, and the southeast conductive zone lies between 40-m and 80-m depth.

The inversion results for the TE-mode data are presented in fig. 11*B*. The results are similar and different in comparison to the TM-mode results in fig. 11*A*. The resistive zone beneath stations 11, 12, 34, 14, and now 16 are clearly divided into two separate resistive zones. The 50 ohm-m zone, between stations 10 and 12, begins at shallower depths (perhaps 10 m deep). The second zone with resistivities of 50–200 ohm-m is beneath stations 34, 14, and 16 and again extends to depth.

A third resistive zone on the southeast end of the line, similar to that observed in the TM-mode data, is more clearly delineated in the TE-mode inversion results. Examination of the section suggests that there may be some periodicity to the resistive zones at depth. The shapes are similar and the centers of the three large resistive zones are regularly separated by approximately 2,000 m. This indicates that they may be related in some fashion through geologic deposition, composition, or structure.

The mixed mode TM/TE inversion modeling results are presented in fig. 11*C*. This figure represents some combination of the resistivity distributions depicted in figs. 11*A* and 11*B*. The general features of both sets of data are clearly delineated. The shallow, near-surface conductive layer is apparent as are the two conductive zones on the northwest and southeast ends of the lines. The central resistive zone beneath stations 10 through 16 in the TM-mode model is clearly separated here into two separate zones with two distinct resistivities. One is beneath stations 9, 10, 11, and 12 between depths of 25 and 60 m with a resistivity of approximately 50 ohm-m. The other is beneath stations 34, 14, 16, and 17, has resistivities ranging from 50 to 200 ohm-m, and extends to at least 300-m depth. The periodicity of the three resistive zones at depth is also observed in these TM/TE results.

In geophysical exploration, verification of an interpretation takes the form of agreement between the results from multiple techniques. One of those multiple techniques usually includes, if they are available, information from borehole logging measurements. The Oakland study area has 16-inch short-normal and 64-inch long-normal borehole resistivity logs available from several test holes close to the AMT profile (fig. 2*B*). Only boreholes 33-EN-07 and 25-EN-07 are almost directly on the profile. The other borehole locations have been orthogonally projected onto the profile and are placed near the closest AMT stations. These are listed in table 8. The 16-inch short-normal borehole resistivity measurements are overlain on the AMT inversion modeling sections shown in fig. 11.

**Table 8.** List of test holes in the Oakland, Nebraska, study area with 16-inch short-normal resistivity logs projected on audio-magnetotelluric (AMT) profile.

| Hole name | Closest AMT station |
|---|---|
| 33-EN-07 | 1 |
| 31-EN-07 | 7 |
| 26-EN-07 | 10 |
| 25-EN-07 | 16 |
| 32-EN-07 | 23 |

The AMT inversion results and those of the borehole resistivity logging generally match quite well taking into account the locations of the test holes relative to the AMT profile. The near-surface resistivities in the borehole logs indicate low electrical resistivities (in the range of 20–30 ohm-m) and the resistivities in the lower sections of the borehole logs generally indicate more resistive material (as much as 100 ohm-m). The AMT sections also indicate low resistivities in the near-surface (in the range of 5–10 ohm-m) and more resistive material at depth (50–100 ohm-m). However, at the bottom of boreholes, the logs indicate generally more conductive material, which is not consistently observed at similar depths in the AMT results. The low resitivity zone is observed in the AMT results near test hole 32-EN-07 but not for 25-EN-07, which is closest to the AMT profile. This would suggest that the geology along the profile exhibits a large degree of lateral heterogeneity. It is also then likely that what could be considered one single paleochannel based only on borehole information in fact probably consists of multiple smaller channels and lenses of more porous alluvium material.

Magnetotelluric impedance polar plots or diagrams provide a measure of MT data dimensionality (Reddy and others, 1977). Figure 12 is a polar plot of stations 14, 16, 25, and

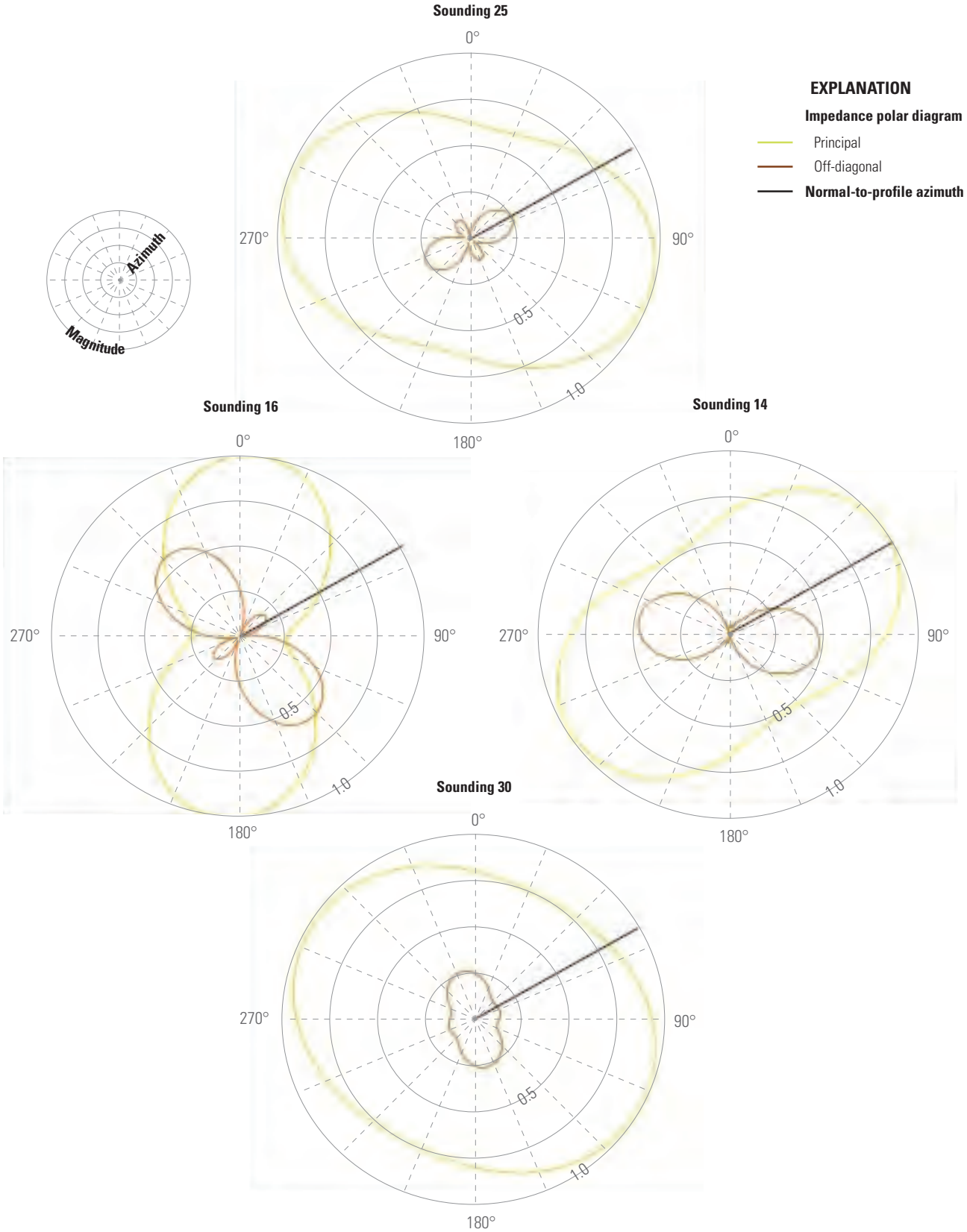


**Figure 12.** Polar diagrams of audio-magnetotelluric soundings, from north to south, stations 25, 16, 14, and 30 at 50 hertz from the Oakland, Nebraska, study area. The principal impedance polar diagram (yellow-green line) elongates either parallel or perpendicular to strike direction. Over resistors, the principal impedance polar diagram elongates perpendicular to strike direction, and over conductors, it elongates parallel to strike direction. For two-dimensional resistivity structures, the off-diagonal impedance polar diagram (brown lines) attains the shape of a symmetric cloverleaf.

30 at 50 Hz. The purpose of this figure is to provide a spatially located comparison of the change in the nature of the polar diagrams along the survey transect. For 1-D resistivity structures, the principal impedance polar diagram (yellow-green line, fig. 12) is a circle. For 2-D or 3-D resistivity structures, the principal impedance polar diagram (yellow-green line) elongates either parallel or perpendicular to strike direction. Over resistors, the principal impedance polar diagram elongates perpendicular to strike direction, and over conductors, it elongates parallel to strike direction. For 2-D resistivity structures, the off-diagonal impedance polar diagram (brown lines, fig. 12) attains the shape of a symmetric cloverleaf. Note that in electromagnetic exploration, high frequencies sample shallow depths and low frequencies sample deeper depths. The ultimate depth of penetration depends on the ground electrical conductivity.

These plots will now be discussed in conjunction with the TM, TE, and TM/TE inversion model results. Beginning with station 30 on the southeast end of the line, the principal impedance polar diagrams (yellow-green lines) indicate predominantly 2-D geology, and the additional impedance polar diagrams (brown lines) indicate a little 3-D character in the subsurface. This is all inferred by the shape of the polar plots. As mentioned in the AMT data analysis section above, over resistors, the principal impedance polar diagrams elongate perpendicular to geologic strike, and over conductors, the principal impedance polar diagrams elongate parallel to the strike direction. At station 30 the principal impedance polar diagram is elongated in a northwesterly direction, which indicates a southwest–northeast geologic strike direction. The additional impedance polar diagrams are generally low in amplitude but do have some small amount of elongation in the north–northwest direction. The polar diagram for station 30 is interpreted as indicating the resistive zone shown in figure 12*C* beneath station 1 and stations farther southeast.

Station 14 sits on about 20 m of conductive material and then resistive material down to at least 300-m depth (fig. 11*C*). The polar diagram (fig. 12) must be interpreted in terms of a conductive material response, and the diagram should be interpreted in terms of a resistive material response. The diagram indicates 2-D structure oriented southwest–northeast and moderate 3-D structure.

There is a substantial change in the character of the structure indicated at stations 14 and 16. Although the near surface regions at both stations are basically 1-D to 2-D, the deeper subsurface at station 16 indicates a much different structure than at station 14 (fig. 12). The polar diagram indicates a very strong 3-D structure is present (larger brown lines of the additional impedance polar diagram) (fig. 12). Whereas the 2-D strike at station 16 is now more northerly in direction, the 3-D structure still has a predominantly southwest to northeast orientation.

The polar diagram at station 25 indicates mostly 1-D to 2-D with almost no 3-D resistivity distributions present (fig. 12). These all correlate very well with what is depicted in the TM-, TE-, and TMTE-mode inversion results (fig. 11).

## Potential Field (Gravity and Magnetic) Results

An airborne geophysical survey of the study area was undertaken in an attempt to map the buried channel system (Abraham and others, 2007). As discussed elsewhere in this report, the airborne electromagnetic system was unable to penetrate the thick conductive till layer forming the topography. In addition to the EM sensors, the airborne system incorporated a precision total field magnetometer. A description and preliminary interpretation of the high-resolution aeromagnetic data it collected is presented later in this section. Also discussed in this section is a study of the feasibility of using airborne gravity or gravity-gradiometer measurements to map the buried channels. The feasibility study, which consisted of 3-D density modeling along with some ground-based gravity profile measurements, was necessary because of the high cost of conducting an airborne gravity survey.

Gravity and magnetic investigations of glacial deposits in this area are complicated by several factors. If they exist at all, the gravity and magnetic anomalies arising from the thickness and compositional variations of the glacial sands and gravels would likely be extremely small. Both gravity and magnetic fields are dominated by high-amplitude, longer wavelength anomalies produced by density and magnetization contrasts in the basement rocks, which are located several hundred meters below the bedrock surface. Lateral variations in the bedrock geology may produce magnetic and gravity anomalies that are significant enough to be detectable by qualitative interpretation methods. The till unit produces a topographic surface that may introduce signal into the aeromagnetic data and will certainly generate up to 90 percent of the signal power in any measured gravity anomaly. Success in removing the topographic signal from the gravity will depend on how uniform the density of the till is and how well this density is known. Finally, the aeromagnetic data are contaminated by short-wavelength anomalies produced by cultural features such as power lines, pipelines, radio towers, and cased boreholes—all of which obscure the signal produced by subtle geologic features. This section first presents the results of the gravity modeling feasibility study, followed by the analysis of the ground-gravity and airborne magnetic-field surveys.

### Gravity Modeling

Radar altimeter and global positioning system data from the airborne geophysical survey (fig. 2) were used to create a digital terrain model for the study area (fig. 13). The total relief of the terrain in this area is 72.35 m. Lithologic logs from ENWRA-drilled test holes (fig. 2) were then used to identify the elevations of the interfaces between the upper till unit, the intermediate sand and gravel unit, and the underlying bedrock shale unit (table 9) relative to the digital terrain model. Grids of these interfaces were created using minimum curvature gridding to extrapolate away from and interpolate between the borehole picks (figs. 14*A* and 14*B*). The bedrock

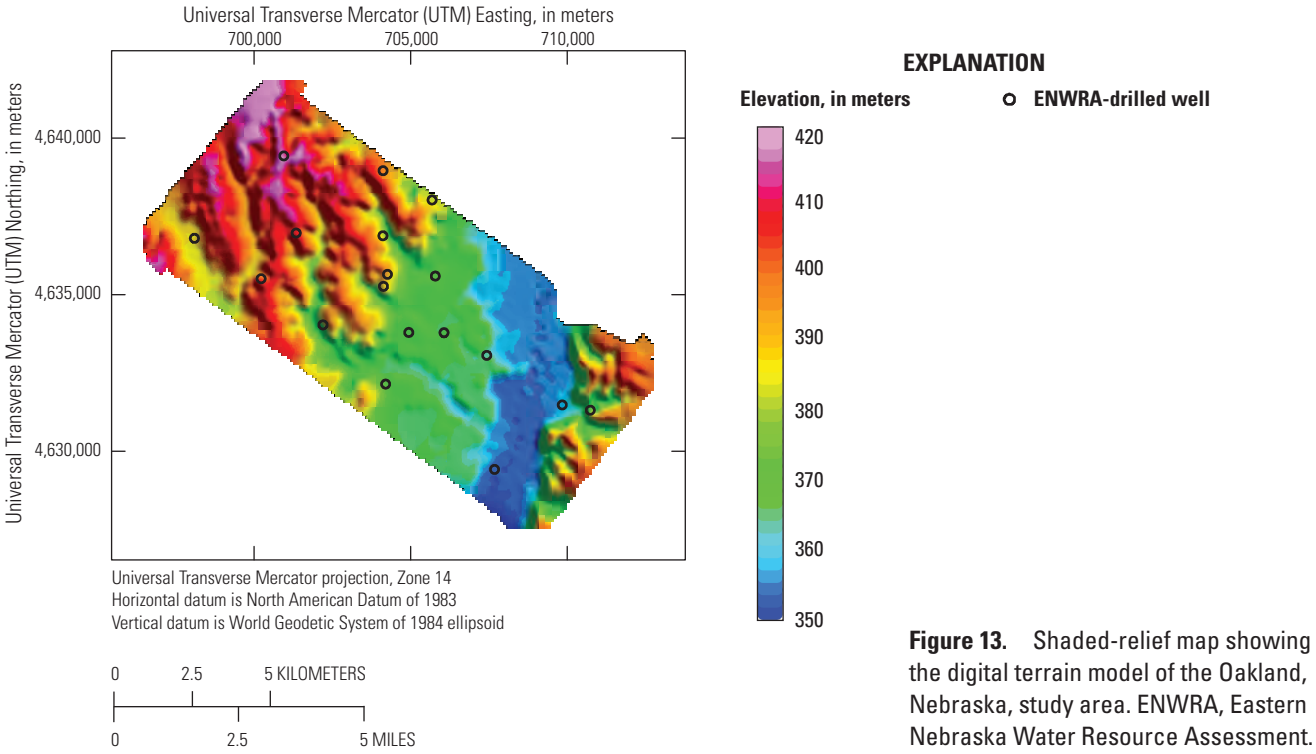


**Figure 13.** Shaded-relief map showing the digital terrain model of the Oakland, Nebraska, study area. ENWRA, Eastern Nebraska Water Resource Assessment.

**Table 9.** Basic borehole data showing picks on the base of till and base of sand for the Oakland, Nebraska, study area.

[In this simplified model, the till unit extends from the ground surface to its base (base till). The sand and gravel unit extends from the base of till to the bedrock surface (base sand)]

| Hole name | Base till elevation (meters) | Base sand elevation (meters) |
|---|---|---|
| 01-EN-06 | 368 | 345 |
| 02-EN-06 | 358 | 345 |
| 03-EN-06 | 337 | 314 |
| 04-EN-06 | 349 | 329 |
| 05-EN-06 | 353 | 345 |
| 22-EN-07 | 365 | 349 |
| 23-EN-07 | 351 | 332 |
| 24-EN-07 | 352 | 323 |
| 25-EN-07 | 358 | 320 |
| 26-EN-07 | 366 | 325 |
| 27-EN-07 | 327 | 324 |
| 28-EN-07 | 348 | 343 |
| 29-EN-07 | 347 | 326 |
| 30-EN-07 | 356 | 309 |
| 31-EN-07 | 350 | 316 |
| 32-EN-07 | 348 | 326 |
| 33-EN-07 | 336 | 323 |

surface (fig. 14*B*) forms a broad, northeast-trending depression through the center of the study area flanked by higher bedrock on the east and northwest. The apparent total relief of the bedrock surface is 42.16 m. Subtracting the bedrock elevation surface from the top-of-sand elevation surface yields the thickness of the sand and gravel unit (fig. 14*C*). The sand and gravel unit is thickest along the northwest side of the bedrock depression, forming a northeast-trending mound or channel that is the target of the geophysical investigations.

The three gridded interfaces—terrain, base of till, and base of sand—were used to create a voxel model of the study area geology. This model was used to calculate theoretical gravity fields on the terrain surface and at aircraft altitude in order to evaluate the feasibility of using ground-based or airborne gravity surveys to map the buried channel deposits. The individual voxel elements measured 25 m by 25 m by 10 m thick. Calculations were done using 3-D Fast Fourier Transforms (Caratori Tontini and others, 2009) and tri-linear interpolation.

Densities were assigned to the till, sand and gravel, and bedrock shale units as shown in table 10 (column 2). The calculated vertical gravity field on the terrain surface (fig. 15*A*) has a range of 4.86 mGal, and is dominated by the effect of the terrain itself. A terrain-corrected gravity field can be calculated by subtracting the gravity field of uniform-density terrain from the uncorrected gravity field. This is equivalent to assigning the densities shown in table 10, column 3 to the model. The terrain-corrected gravity field on the terrain

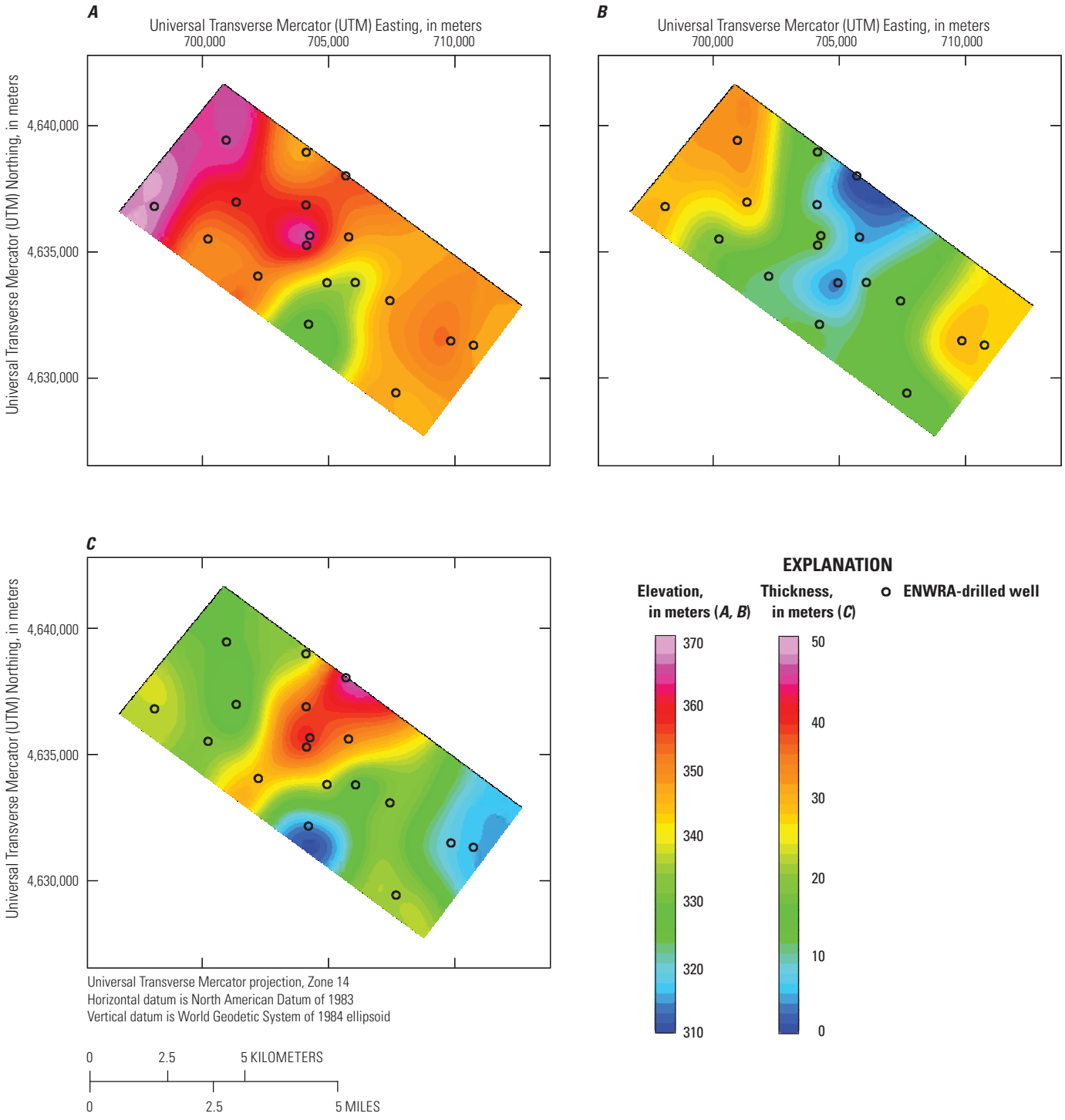


**Figure 14.** Maps of the Oakland, Nebraska, study area showing the elevation of *A*, base of till (or top of sand) and *B*, base of sand (or bedrock surface) as estimated from lithologic data from Eastern Nebraska Water Resource Assessment (ENWRA) drilled wells using minimum-curvature gridding; *C*, sand thickness (isopach) is estimated using the till and sand bases.

**Table 10.** Density values assigned to the gravity model for the Oakland, Nebraska, study area.

[g/cm³, gram per cubic centimeter]

| Material | Actual assigned density (g/cm³) | Ideal terrain-corrected density contrasts (g/cm³) | Standard terrain-corrected density contrasts (g/cm³) |
|---|---|---|---|
| Air | 0.00 | 0 | 0 |
| Dry till | 1.95 | 0 | –.72 |
| Wet sand | 2.05 | 0.1 | –.62 |
| Shale | 2.25 | 0.3 | –.42 |

surface (fig. 15*B*) has a range of only 0.40 mGal, and is dominated by the signal produced by the bedrock surface. The target sand and gravel channel does not produce an obvious gravity signal. The terrain-corrected vertical gravity gradient, calculated on the terrain surface (fig. 15*C*), also fails to image the thickened sand unit. At a typical aircraft altitude, such as 152 m above the mean terrain, the gravity effect of the sand thickness variations will be greatly reduced. For a linear feature, the gravity field decays as one over the distance, and the vertical gravity gradient decays as one over the distance squared.

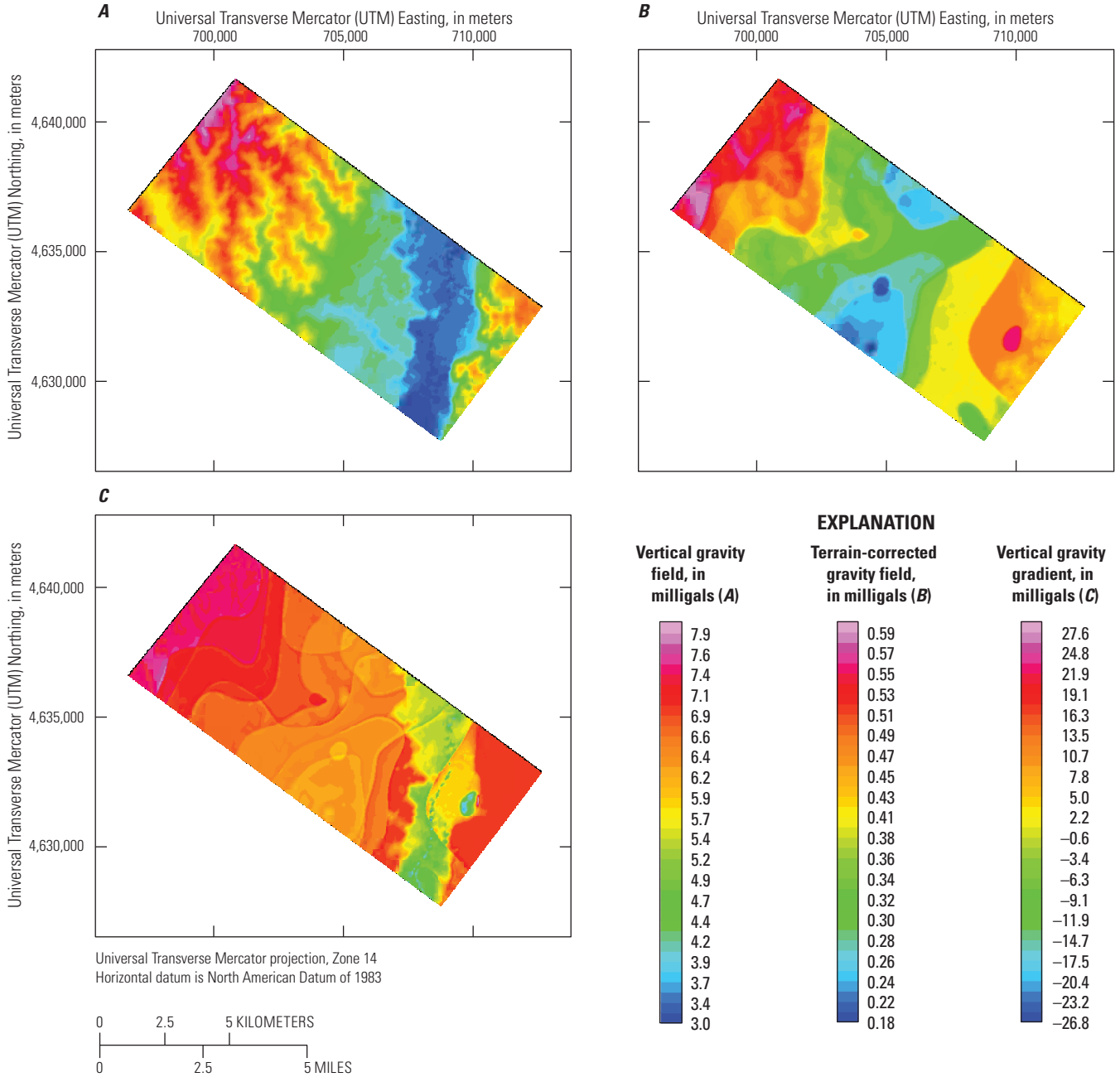


**Figure 15.** Maps of the Oakland, Nebraska, study area showing *A*, calculated vertical gravity field on the terrain, *B*, calculated terrain-corrected gravity on the terrain (this is the estimated gravity field of the sand unit and the underlying bedrock), and *C*, calculated terrain-corrected vertical gravity gradient on the terrain. The apparent stepping is an artifact of the 10-meter vertical resolution of the density voxel model.

## Gravity Survey

Available gravity data for the Oakland study area include regional gravity station data and a gravity profile collected on the ground across the target paleochannel as part of this study (figs. 2 and 16). This profile followed a drainage in order to minimize the effect of terrain on the gravity data. The gravity-station spacing along the profile was 250 m. Eleven regional gravity stations exist within the boundary of the study area (shown as black plus symbols in fig. 16). Additional stations lie just outside the study area. The regional gravity field is dominated by elliptical gravity highs produced by dense mafic rocks in the Precambrian basement.

The complete Bouguer gravity anomaly was computed using a standard density of 2.67 g/cm$^3$ for the terrain correction (fig. 16). The resulting gravity profile displays a 9-mGal linear trend that follows that of the regional gravity field. After removal of this trend, the residual gravity anomalies have an amplitude range of less than 2 mGal (fig. 17*A*). This residual gravity field does not show any obvious correlation with the target sand and gravel body as modeled using the borehole data (model 1). Applying the standard terrain-corrected density contrasts (table 10, column 4), the calculated field of model 1 has a root-mean-squared misfit of over 0.5 mGal (fig. 17*B*).

In order to reproduce the residual gravity field using relief on the bedrock surface, nearly 100 m of relief would be required if a large density contrast of 0.5 g/cm$^3$ was used (model 2, fig. 17*C*). A more realistic density contrast of 0.2 or 0.3 g/cm$^3$ would require around 200 m of relief on the bedrock surface. The borehole data do not support bedrock relief of more than 50 m within the study area. It follows that the residual gravity field along the profile is most likely produced primarily by density variations within the bedrock, with secondary contributions from the overlying sand-gravel and till units. Because the scale and distribution of density variations within the bedrock units are completely unknown, meaningful interpretation of sand and gravel thickness variations from a ground-based microgravity survey would likely prove impossible.

## Magnetic Survey

As part of the airborne geophysical survey, aeromagnetic data were collected along flight lines spaced 250 m apart (fig. 2) and at a ground clearance of about 30 m. The gridded aeromagnetic data (fig. 18) display a combination of high-amplitude, long-wavelength anomalies produced by geologic sources at depth and short-wavelength anomalies produced by cultural sources, such as wells and power lines. Due to the extremely low altitude and wide flight-line spacing, the anomalies due to cultural sources are badly aliased by the gridding. These anomalies appear to have power at unrealistically long wavelengths, and thus are difficult to separate from anomalies generated by geologic sources at bedrock depths.

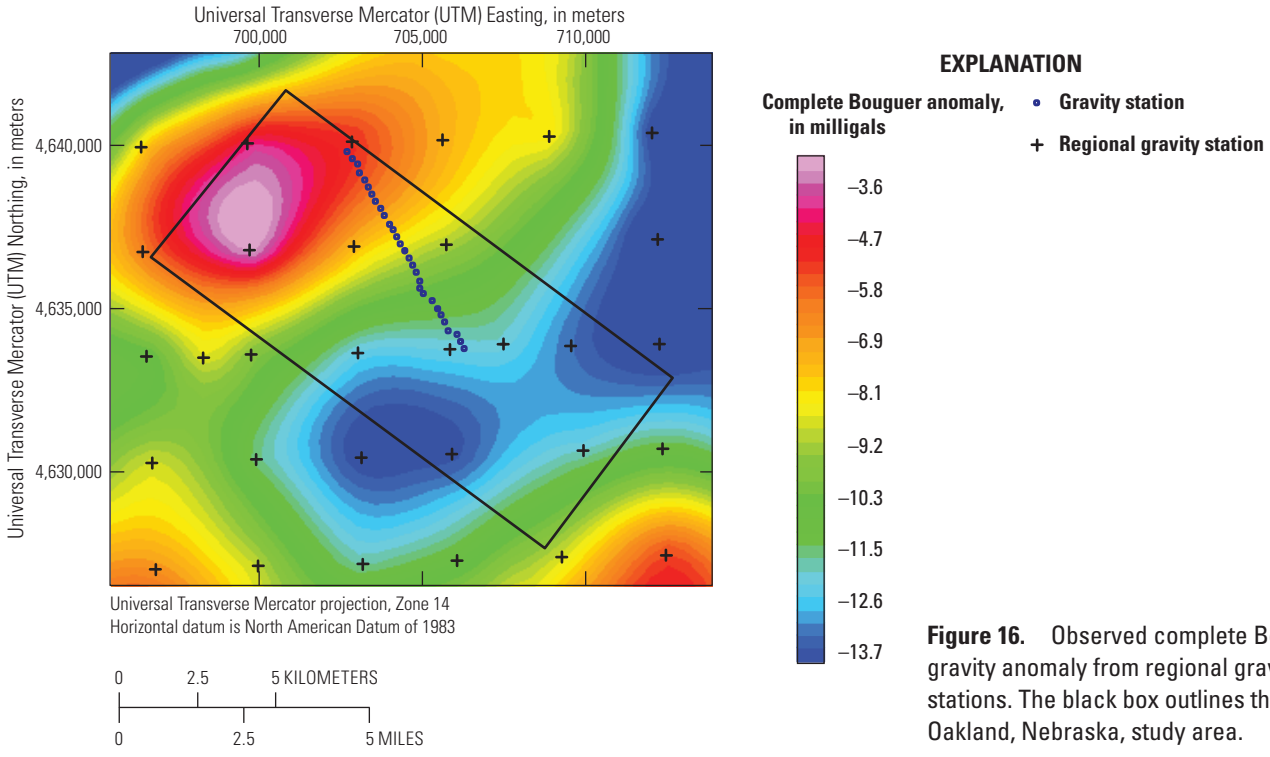


**Figure 16.** Observed complete Bouguer gravity anomaly from regional gravity stations. The black box outlines the Oakland, Nebraska, study area.

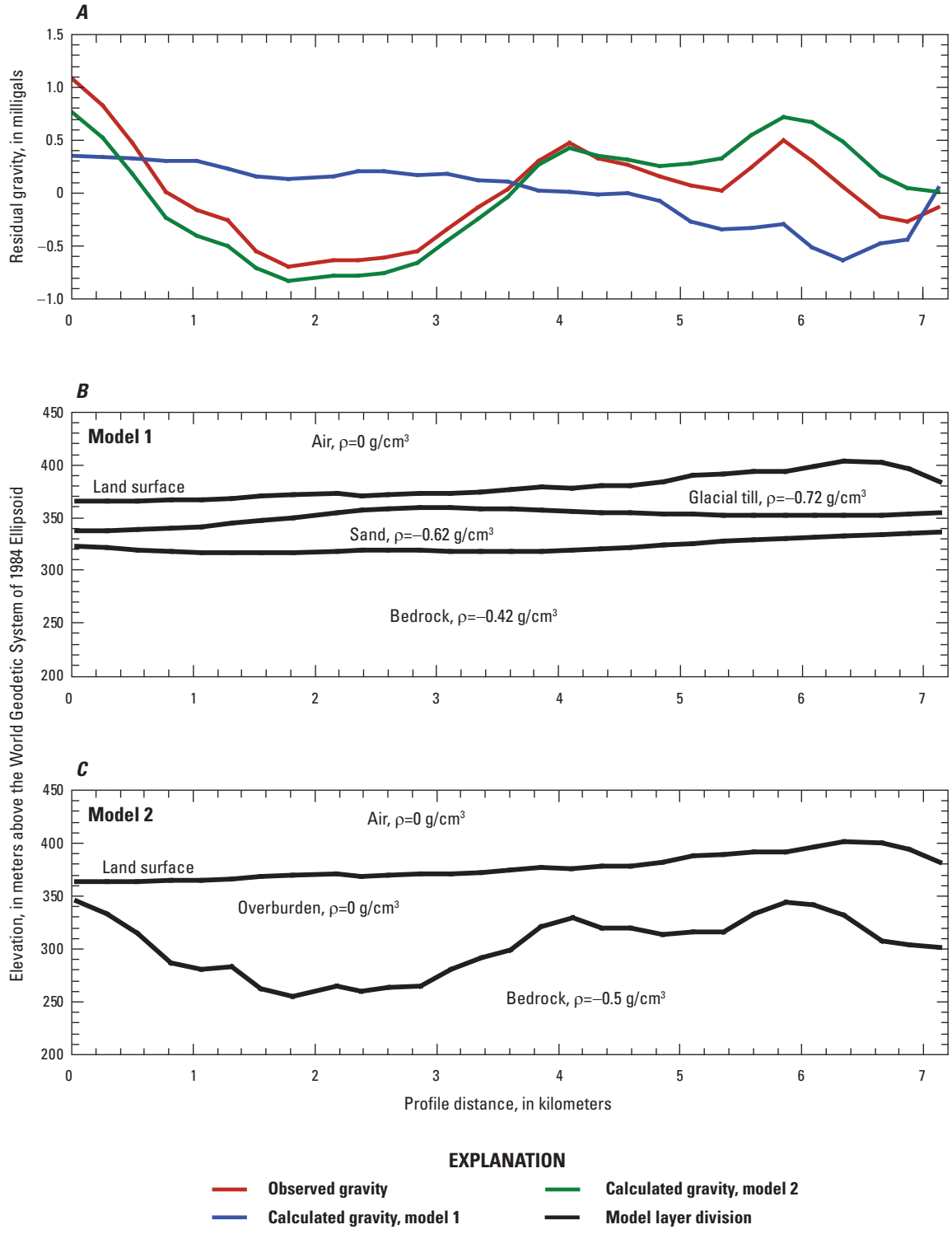


**Figure 17.** Graphs showing *A*, observed gravity profile and calculated gravity profiles from *B*, density model based on the lithologic data from the Eastern Nebraska Water Resource Assessment drilled test holes (model 1), and *C*, idealized density model that attempts to recreate the observed gravity profile (model 2). The standard terrain-corrected density contrasts are shown for each model layer. The relief of model 2 bedrock surface would be even greater if a more realistic (lower) bedrock density contrast was used. ρ, densities; g/cm³, gram per cubic centimeter.

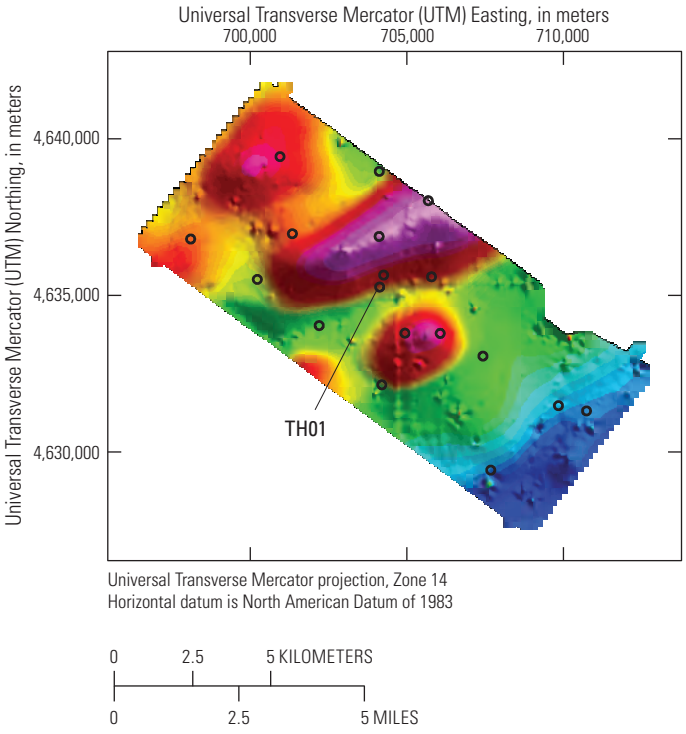


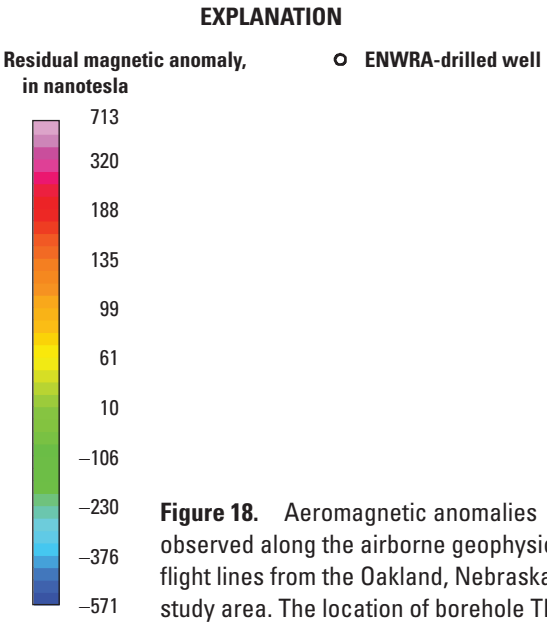


**Figure 18.** Aeromagnetic anomalies observed along the airborne geophysical flight lines from the Oakland, Nebraska, study area. The location of borehole TH01 is indicated. ENWRA, Eastern Nebraska Water Resource Assessment.

The long-wavelength magnetic anomalies are similar to regional gravity anomalies attributed to mafic rocks in the Precambrian basement. However, the magnetic anomalies do not correspond directly to the gravity anomalies, and some of the highest amplitude magnetic anomalies occur over parts of the sand and gravel channel. In order to eliminate the possibility that the long-wavelength magnetic anomalies are produced by extremely magnetic sands at shallow depth, magnetic susceptibility measurements were made on cuttings from borehole TH01 (shown on fig. 19). The magnetic susceptibility measurements (fig. 19) demonstrate that that the sand and gravel units are essentially nonmagnetic, and the overlying till units are only slightly magnetic.

In order to further investigate the distribution of magnetic sources with depth, matched bandpass filtering (Syberg, 1972; Phillips, 2001) was applied to the gridded aeromagnetic data. The matched filtering approach involves constructing a mathematical model out of equivalent magnetic layers, such that the power spectrum of the model matches the power spectrum of the aeromagnetic data. Each equivalent layer in the model corresponds to a bandpass filter, which when applied to the aeromagnetic data, reveals the portion of the magnetic field produced at the depth of the equivalent layer.

The results of matched bandpass filtering will depend on the number and type of equivalent layers used to fit the power spectrum. Layers may be either thin “dipole” layers or thick magnetic half-spaces. Because the finite widths of the magnetic sources are ignored, depths to the equivalent layers are usually overestimates of the true depth. Normally, the power spectrum of an aeromagnetic dataset should be modeled using one or more thin equivalent layers at shallow depth to fit the flight-line noise and the cultural sources, and one or

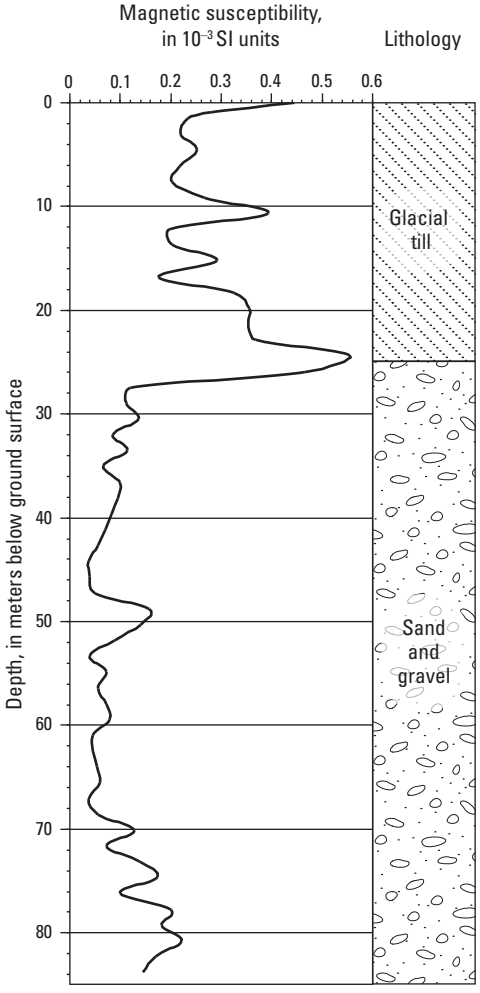


**Figure 19.** Magnetic susceptibility measurements on cuttings from borehole TH01.

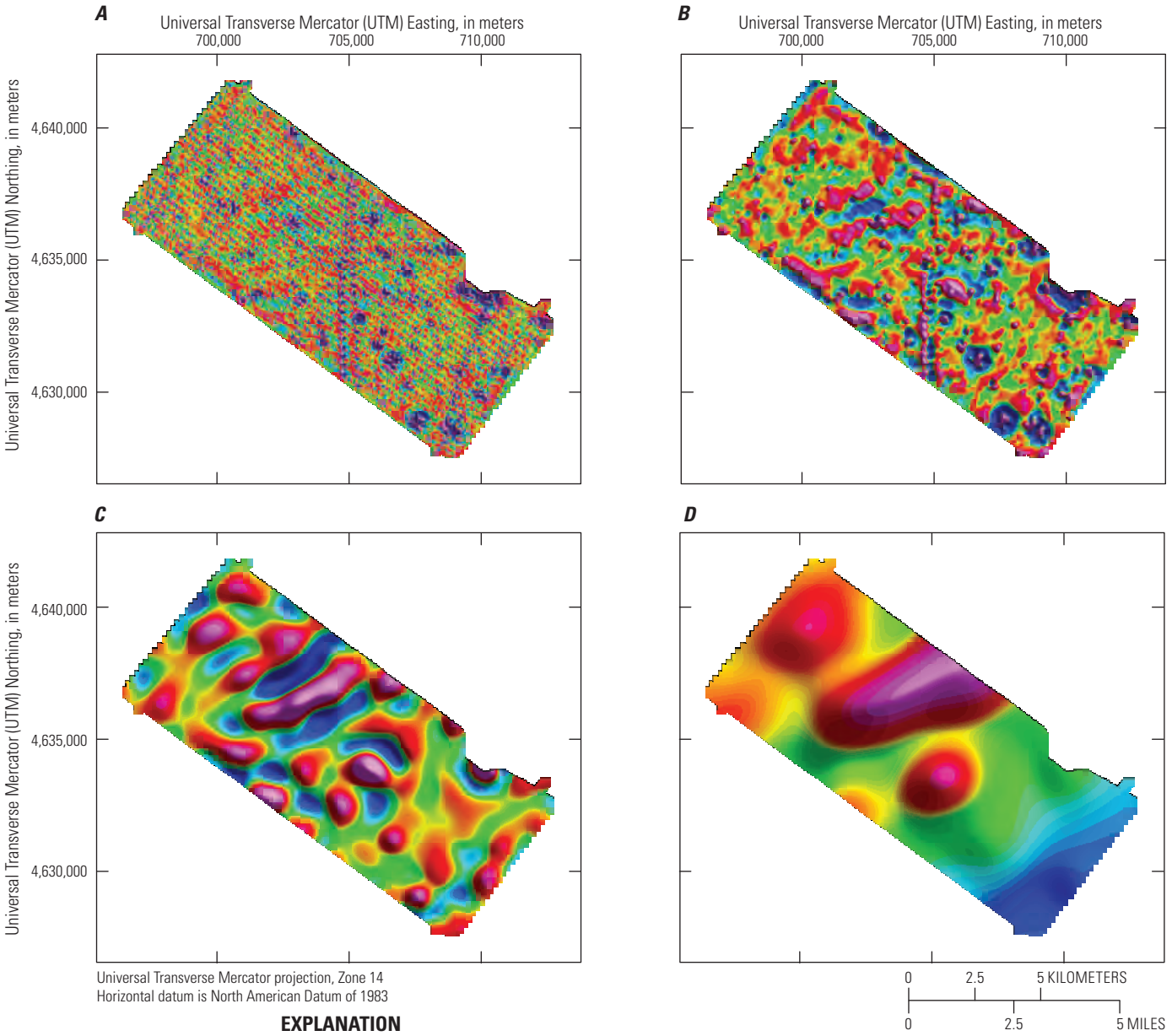


**Figure 20.** Shaded-relief maps of the Oakland, Nebraska, study area showing *A*, highpass-filtered aeromagnetic anomalies produced near the ground surface, *B*, bandpass-filtered aeromagnetic anomalies produced near an equivalent depth of 98 meters (these may represent the aliased long wavelengths from the cultural anomalies as well as any magnetic signals from the bedrock surface), *C*, bandpass-filtered aeromagnetic anomalies produced near an equivalent depth of 620 meters (the amplitudes of these anomalies suggest that they represent the shorter wavelength components of anomalies produced by Precambrian basement sources), and *D*, lowpass-filtered aeromagnetic anomalies produced near an equivalent depth of 1,956 meters (these represent the longer wavelength anomalies produced by sources at the Precambrian basement surface).

more magnetic half-spaces at greater depth to fit the geologic sources. In the case of the Oakland aeromagnetic data, the aliasing of the cultural anomalies required that magnetic half-spaces be used for all the equivalent layers. Four equivalent layers were used, at depths of 24, 98, 620, and 1,956 m below the flight surface. The magnetic anomalies produced by the 24-m equivalent layer (fig. 20*A*) represent the residual flight-line noise, the short-wavelength cultural anomalies, and any magnetic signal from the glacial till, which forms the topographic surface. Topographic anomalies are not apparent, indicating that the till is not a significant magnetic source. The magnetic anomalies produced by the 98-m equivalent layer (fig. 20*B*) represent the aliased long wavelengths from the cultural anomalies as well as any magnetic signals from the bedrock surface. Magnetic sources in the bedrock appear to strike east–west and east–northeast in the northern part of the study area. A northeast-trending magnetic channel system may be present within the bedrock in the southeast third of the area. The magnetic anomalies produced by equivalent layers at depths of 620 and 1,956 m (fig. 20*C*, 20*D*) likely represent sources near the Precambrian basement surface.

## Summary and Discussion

The U.S. Geological Survey performed surface geophysical surveys along a 7-km transect over a presumed paleochannel in a study area west of Oakland, Nebraska, which was the subject of a helicopter electromagnetic study in 2007. Because of very limited groundwater resources in this region, improved hydrogeologic mapping and characterization techniques are needed to delineate aquifers, assess their degree of hydrologic connection with streams and other aquifers, and better predict water quality and quantity. The objectives of the surveys were to evaluate and compare the capabilities of several geophysical methods—time-domain electromagnetic (TDEM), audio-magnetotelluric (AMT), gravity, and magnetic field—to detect and delineate paleochannels in the glacial deposits of eastern Nebraska.

The HEM method proved to have insufficient depth of penetration to reveal buried paleochannels. The TDEM and AMT methods achieved sufficient depth of penetration, but did not detect the assumed 1-km-wide paleochannel. It is also then likely that what could be considered one single paleochannel based only on borehole information, in fact, probably consists of multiple smaller channels and lenses of more porous alluvium material. Simulated gravity anomalies indicate that thickening of an important sand and gravel aquifer near Oakland, Nebraska, would be difficult to detect using ground-based or airborne gravity measurements. Even with perfect correction for terrain effects, the gravity anomaly produced by the thickness variations observed in boreholes would only have an amplitude of 0.4 mGal at the ground surface.

TDEM measurements reveal subsurface resistivity structure to depths of 200 m. Inversion of data along a 7-km profile define a layer of conductive glacial till of variable thickness (15–40 m) atop a layer of variable resistivity that represents a volume average of gravel and sand, one or more clay and shale layers, and a deeper sandstone layer, as defined in part by lithologic data. All the above overlie a flat-lying conductive horizon at 130-m depth, attributed to a clay-shale unit within the Cretaceous Dakota Formation. Although the TDEM models are unable to define the geometry of the sand-gravel package, they do indicate an increase in resistivity that is spatially coincident with the package. Thus TDEM measurements offer the ability to identify resistive regions beneath thick glacial till that may be related to sand and gravel lenses or paleochannels. Sensitivity studies modeled upon commercial airborne TDEM systems suggest that such resistive lenses or paleochannels are resolvable beneath thick conductive till to depths of 100–150 m. Such modeling is idealized and does not account for system bias, cultural noise, spatial aliasing, and the effects of incomplete or erroneous system characterization (sensor altitude and orientation, system filters, and relative timing). The spatial coverage offered by airborne systems, however, provides opportunities to identify resistive lenses and (or) paleochannels that cannot be easily discerned from limited ground data.

After correction for the regional gravity field, a gravity profile measured across the thickened sand and gravel unit displays a residual amplitude range of less than 2 mGal. The residual anomalies are uncorrelated with the thickened aquifer unit and cannot be explained by the observed relief on the bedrock surface, and most likely are produced by density variations within the bedrock shale units. Any such bedrock density variations would further impede detection of the thickened aquifer unit using gravity measurements.

Magnetic susceptibility measurements on borehole cuttings indicate that the sand and gravel unit is effectively nonmagnetic, and the overlying till unit is only weakly magnetic. High-resolution aeromagnetic data collected 30 m above ground are dominated by high-amplitude, long-wavelength anomalies produced at the Precambrian basement surface and short-wavelength anomalies produced by cultural sources near the ground surface. Filtered aeromagnetic anomalies indicate no contributions from geologic units above the bedrock surface, and only weak contributions from susceptibility variations within the bedrock shales.

Based on these results, neither gravity measurements nor magnetic measurements are likely to detect the thickened aquifer unit that is the target of these investigations.

According to forward models TDEM and AMT should have located a paleochannel in the glacial till deposits. If a paleochannel exists in the study area, it is probably in the Dakota Formation underlying the glacial till deposits, and it probably does not intersect the geophysical transect.

## Future Work

This research was focused on identifying a geophysical technique capable of detecting the aquifers within the heavy tills of eastern Nebraska. The Oakland area was chosen as a

test area for the evaluation of four geophysical methods. Of the methods that were evaluated, TDEM has the ability to be deployed from an airborne platform. Airborne TDEM methods have found considerable use throughout the world (Auken and others, 2007; Fountain, 2008; Siemon and others, 2009). Airborne methods are particularly useful for mapping large areas in a time efficient manner.

In order to evaluate the suitability of the airborne platform to identify the location of aquifers within the heavy tills of eastern Nebraska, a numerical study was performed using Earth models derived from the ground TDEM that was collected over the Oakland study area. Three electrical Earth models were utilized in this numerical modeling study: (1) southern end of the TDEM profile, (2) center of the TDEM profile, and (3) north end of the TDEM profile (table 11) (fig. 21).

Two general airborne TDEM systems were modeled that would perform moderately well in the environment of the heavy tills of eastern Nebraska. These systems do not represent specific single commercial systems but are representative of several of the systems available and represent their capabilities (table 11). Airborne system 1 represents a collection of systems that are typically found in the mineral exploration industry. Airborne system 2 represents a collection of systems that are designed for near-surface characterizations and typically found in groundwater studies.

As a comparison, the electrical Earth models were modeled using a ground TDEM system configuration (fig. 21). The ground system indicates that the response curves (two curves from each model due to duty cycle from modeled ground system) from the three models indicate a low resistivity (northern model), moderate resistivity (central model), and low resistivity (southern model). To simulate actual data more accurately, 10-percent noise was added to the signals and is represented as error bars in figure 21*B*. For the ground modeling, a clear separation can be seen in the response curves from the central model from both the northern and the southern models. There is no clear separation between the northern and southern model. The modeling of the ground TDEM system is solely to serve as a reference for the airborne system modeling results. Results of modeling airborne system 1 indicate that there is a detectable separation in the response curves between the central model and both northern and southern models (fig. 21). As with the ground system, there is no detectible difference in the northern and southern models. Results of modeling airborne system 2 indicate that there is a detectable separation in the response curves between the central model and both the northern and southern models (fig. 21). As with the ground system and airborne system 1, there is no detectible difference in the northern and southern models. All modeling results are indicating that the electrical Earth models from the central area of the Oakland TDEM profile can be distinguished from both the northern and southern ends.

Although the detection of the moderate resistivity zone represented by the central model is achievable at the surface and by both systems modeled, it needs to be cautioned that due to the non-uniqueness of the inversions, accurately modeling the thickness and absolute resistivity of the moderate resistivity layer is unlikely. As explained in the above section on the TDEM method, the resolution of resistors is much more challenging than detecting conductive features. Due to the low electrical resistivity contrast of the sand and gravel deposits within the central section of the Oakland TDEM profile, it is unlikely that without additional data (resistivity of the materials from borehole measurements) those inversions of airborne data could accurately determine the layer thickness. This is not all bad news because the modeling effort, as well as the ground-data collection, show that the detection of the lateral position of these sand and gravel deposits are achievable from an airborne TDEM system.

Based upon the analysis and interpretation of the four methods evaluated and the numerical modeling of the airborne TDEM system, future work could include large-scale reconnaissance survey using a well-calibrated TDEM airborne system. This method would

a. achieve sufficient depth of penetration,

b. have high signal-to-noise ratio,

c. provide calibrated, quantitative, invertible data, and

d. allow spatial correlation of conductivity anomalies.

**Table 11.** General system characteristics of modeled airborne time-domain electromagnetic systems.

[Hz, hertz; A, amp; $m^2$, square meter; m, meter; µs, microsecond; ms, millisecond; LM, low moment; HM, high moment]

| System | Type | Waveform | Base frequency (Hz) | Spectrum | Number of turns | Current peak (A) | Transmitter area ($m^2$) | Moment (A-$m^2$) | Sensor height average (m) |
|---|---|---|---|---|---|---|---|---|---|
| Airborne system 1 | Rigid frame central loop receiver | Bipolar triangular wave | 90 | 58 µs to 3.2 ms | 5 | 397 | 460 | 237,000 | 48 +/- 8 |
| Airborne system 2 | Rigid frame null-coupled Z receiver, dual moment | Bipolar square wave | 30 | 10 µs to 7 ms | 1 (LM)<br>4 (HM) | 10<br>100 | 314<br>314 | 3,000<br>120,000 | 32 +/- 5 |

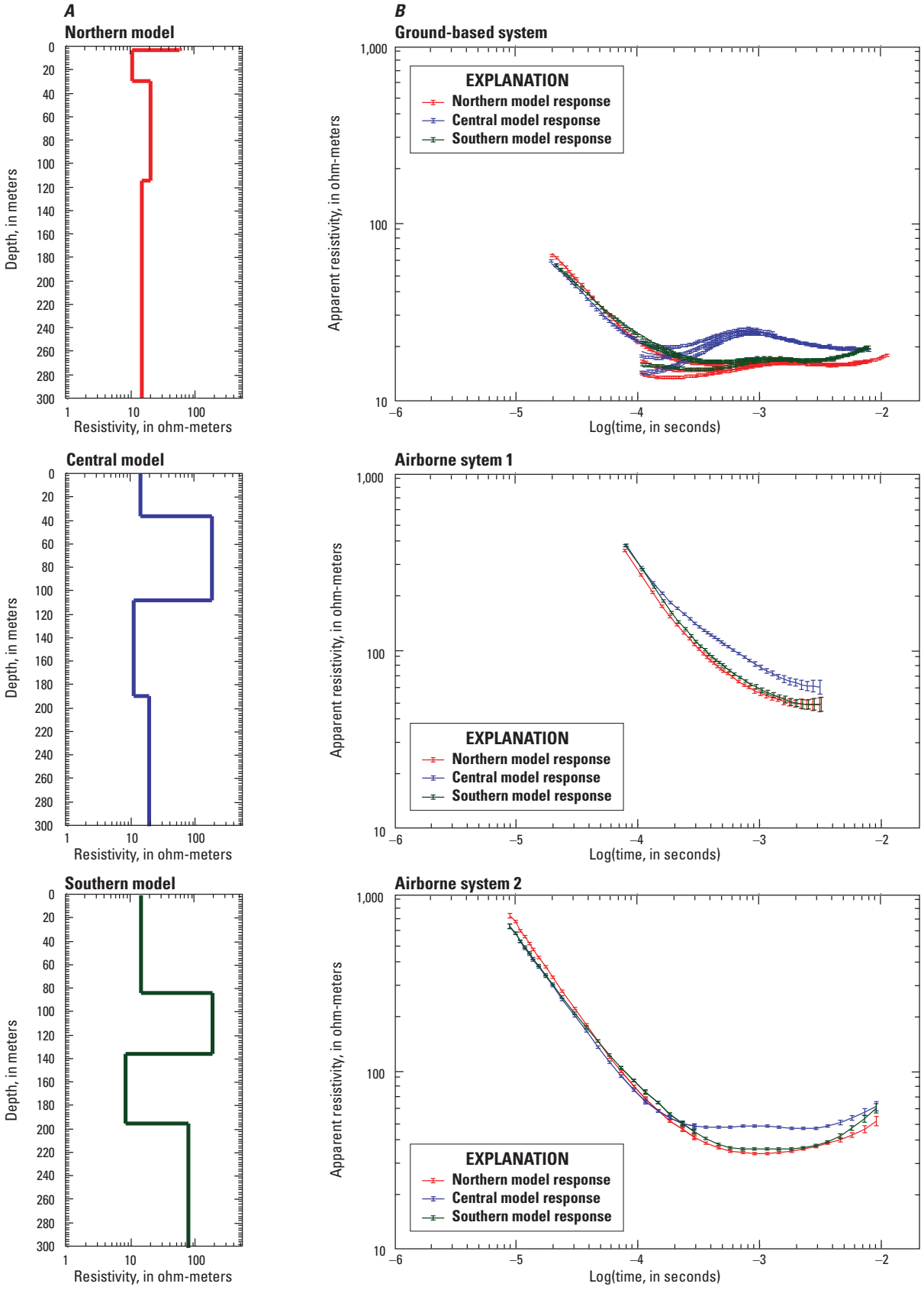


**Figure 21.** Time-domain electromagnetic forward modeling results for the Oakland, Nebraska, study area. *A*, Three characteristic electrical models for the northern, central, and southern parts of the study area and *B*, forward model responses of ground-based airborne system 1 and airborne system 2 .

## References Cited


Abraham, J.D., Cannia, J.C., Smith, B.D., Steele, G.V., and Korus, J.T., 2007, Preliminary results of hydrogeological framework studies of surface water-groundwater systems in eastern Nebraska using airborne and ground geophysics [abs.]: Geological Society of America Annual Meeting, Abstracts with Programs, v. 39, no. 6, p. 162.

Auken, E., and Nebel, K., 2001, Getting started with SiTEM and SEMDI: Hydro Geophysics Group, University of Aarhus, Denmark, 22 p., available at *http://www.aarhusgeo.com/download/software-manuals.html*.

Auken, E., Westergaard, J.A., Christiansen, A.V., and Sørensen, K.I., 2007, Processing and inversion of SkyTEM data for high-resolution hydrogeophysical surveys: Presented at the 19th International Geophysical Conference and Exhibition, ASEG, Perth, Western Australia, 2 p., available at *http://www.aarhusgeo.com/Publications/conference-proceedings-and-presentations.html*.

Bentall, R., University of Nebraska-Lincoln, Conservation and Survey Division, Nebraska Department of Water Resources, and U.S. Geological Survey, 1971, Water supplies and the land, the Elkhorn River basin of Nebraska: Lincoln, Nebr., University of Nebraska-Lincoln, Conservation and Survey Division Resource Atlas no. 1, 51 p.

Blakely, R.J., 1996, Potential theory in gravity and magnetic applications: New York, Cambridge University Press, 441 p.

Burchett, R.R., and Smith, F.A., 1991, Burt County test-hole logs: Lincoln, Nebr., University of Nebraska–Lincoln, Conservation and Survey Division, Water Survey Test-Hole Report No. 11, 35 p.

Burchett, R.R., and Smith, F.A., 1993, Cuming County test-hole logs: Lincoln, Nebr., University of Nebraska–Lincoln, Conservation and Survey Division, Water Survey Test-Hole Report No. 20, 56 p.

Caratori Tontini, F., Cocchi, L., and Carmisciano, C., 2009, Rapid 3-D forward model of potential fields with application to the Palinuro Seamount magnetic anomaly (southern Tyrrhenian Sea, Italy): Journal Geophysical Research, v. 114, B02103, doi:10.1029/2008JB005907.

Christiansen, A.V., and Christensen, N.B., 2003, A quantitative appraisal of airborne and ground-based transient electromagnetic (TEM) measurements in Denmark: Geophysics, v. 68, p. 523–534.

Danielsen, J.E., Auken, E., Jørgensen, F., Søndergaard, V., and Sørensen, K.I., 2003, The application of the transient electromagnetic method in hydrogeophysical surveys: Journal of Applied Geophysics, 53, p. 181–198.

Dobrin, M.D., and Savit, C.H., 1988, Introduction to geophysical prospecting (4th ed.): New York, McGraw-Hill, 867 p.

Dransfield, M., Roux, T.L., and Burrows, D., 2010, Airborne gravimetry and gravity gradiometry at Fugro Airborne Surveys, *in* Lane, R.J.L., ed., Airborne gravity 2010—Abstracts from the ASEG-PESA airborne gravity workshop: Published jointly by Geosciences Australia and the Geological Survey of New South Wales, Geoscience Australia Record 2010.23 and GSNSW File GS2010/0457, p. 49–57.

Eberhart-Phillips, D., Stanley, W.D., Rodriguez, B.D., and Lutter, W.J., 1995, Surface seismic and electrical methods to detect fluids related to faulting: Journal of Geophysical Research, v. 100, p. 12919–12936.

Egbert, G.D., 1997, Robust multiple station magnetotelluric data processing: Geophysics Journal International, v. 130, p. 475–496.

Ellis, M.J., 1984, Overview of the Dakota aquifer system in Nebraska, *in* Geohydrology of the Dakota aquifer, Lincoln, Nebraska: Dublin, Ohio, National Water Well Association, p. 48–55.

Farquharson, C.G., 2000, Background for program "EM1DFM," v. 1.0: Vancouver, British Columbia, Canada, University of British Columbia Geophysical Inversion Facility, 20 p.

Farquharson, C.G., and Oldenburg, D.W., 2004, A comparison of automatic techniques for estimating the regularization parameter in non-linear inverse problems: Geophysical Journal International, v. 156, p. 411–425.

Fitterman, D.V., 1988, Examples of transient soundings for ground-water exploration in sedimentary aquifers: Groundwater, v. 25, p. 685–692.

Fitterman, D.V., and Labson, V.F., 2005, Electromagnetic induction methods for environmental problems, *in* Butler, D.K., ed., Near surface geophysics: Tulsa, Okla., Society of Exploration Geophysicists, SEG Investigations in Geophysics Series No. 13, p. 301–355.

Fitterman, D.V., and Stewart, M.T., 1986, Transient electromagnetic sounding for groundwater: Geophysics, v. 51, p. 995–1005.

Fountain, D., 2008, 60 years of airborne EM—Focus on the last decade, Proceeding on AEM2008: Presented at the 5th International Conference on Airborne Electromagnetics, 28–30 May 2008, Hotel Haikko, Finland, 11 p.

Flowerday, C.A., Kuzelka, R.D., and Pederson, D.T., 1998, The groundwater atlas of Nebraska (RA-4a): Lincoln, Nebr., University of Nebraska at Lincoln Conservation and Survey Division, 44 p.

Fugro Airborne Surveys Corp., 2007, Resolve survey for U.S. Geological Survey—Oakland, Ashland, and Firth survey areas, Fremont, Nebraska: Mississauga, Ontario, Canada, Fugro Airborne Surveys Corp., May 25, 2007, 72 p.

Gamble, T.D., Goubau, W.M., and Clarke, J., 1979, Error analysis for remote reference magnetotellurics: Geophysics, v. 44, no. 5, p. 959–968.

Geological Institute, 2002a, Vejledning i kalibrering af TEM måleudstyr (in Danish): Aarhus University, 12 p.

Geological Institute, 2002b, Test og sammenligning af Transient Elektromagnetiske instrumenter i Danmark (in Danish): Aarhus University, 118 p.

Geometrics, 2007, STRATAGEM 26716-01 Rev. F, Operation manual for systems running IMAGEM ver. 2.19: Geometrics, Inc., 45 p.

Geotools, 1998, Geotools MT user's guide: Geotools Corporation, a division of AOA Geophysics, 450 p.

Gosselin, D.C., Headrick, J., Chen, X.H., Summerside, S.E., Tremblay, R., and Bottger, K., 1996, Domestic water-well quality in rural Nebraska: Lincoln, Nebr., University of Nebraska–Lincoln, Conservation and Survey Division, Open-File Report 52, 155 p.

High Plains Regional Climate Center, 2011, Historical climate data summaries: Lincoln, Nebr., University of Nebraska-Lincoln, accessed September 2011 at *http://www.hprcc.unl.edu/data/historical/index.php*.

Kearey, P., and Brooks, M., 1991, An introduction to geophysical exploration, 2nd ed.: Boston, Mass., Blackwell Scientific Publications, 254 p.

Keller, G.V., 1987, Rock and mineral properties, *in* Nabighian, M.N., ed., Electromagnetic methods in applied geophysics theory: Tulsa, Okla., Society of Exploration Geophysicists, v. 1, p. 13–51.

Keller, G.V., 1989, Electrical properties, *in* Carmichael, R.S., ed., Practical handbook of physical properties of rocks and minerals: Boca Raton, Fla., CRC Press, p. 359–427.

Kenny, J.F., Barber, N.L., Hutson, S.S., Linsey, K.S., Lovelace, J.K., and Maupin, M.A., 2009, Estimated use of water in the United States in 2005: U.S. Geological Survey Circular 1344, 52 p.

Korus, J.T., and Divine, D., 2007, The eastern Nebraska water resources assessment (ENWRA) [abs.]: Geological Society of America Annual Meeting, Abstracts with Programs, v. 39, no. 6, p. 525.

Lane, R., Smith, R., Dransfield, M., and Robson, D., 2010, Introduction to "Airborne Gravity 2010," *in* Lane, R.J.L., ed., Airborne gravity 2010—Abstracts from the ASEG-PESA airborne gravity workshop: Published jointly by Geosciences Australia and the Geological Survey of New South Wales, Geoscience Australia Record 2010.23 and GSNSW File GS2010/0457, p. 1–4.

Lawton, D.R., Goodenkauf, O., Hanson, B.V., and Smith, F.A., 1984, Dakota aquifers in eastern Nebraska—Aspects of water quality and use, *in* Jorgensen, D.G., and Signor, D.C., eds., Geohydrology of the Dakota aquifer—Proceedings of the C.V. Theis conference on geohydrology: Worthington, Ohio, National Water Well Association, p. 221–228.

Lipinski, B.A., 2007, Integrating geophysics and geochemistry to evaluate coalbed natural gas produced water disposal, Powder River Basin, Wyoming: Pittsburg, Pa., University of Pittsburg, Ph.D. dissertation, 110 p.

Mackie, R., Rieven, S., and Rodi, W., 1997, User's manual and software documentation for two-dimensional inversion of magnetotelluric data: GEOTOOLS MT User's Guide RLM2DI Supplement, 10 p.

Mason, J.A., Joeckel, R.M., and Bettis, E.A., 2007, Middle to late Pleistocene loess record in eastern Nebraska, USA, and implications for the unique nature of oxygen isotope stage 2: Quaternary Science Reviews, v. 26, no. 5–6, p. 773–792.

Murphy, C.A., and Brewster, J., 2007, Target delineation using full tensor gravity gradiometry data [abs.]: Extended Abstract, ASEG-PESA 19th International Geophysical Conferences and Exhibition, Perth, Australia, 2007, 3 p.

Murphy, C.A., 2010, Recent developments with Air-FTG, *in* Lane, R.J.L., ed., Airborne gravity 2010—Abstracts from the ASEG-PESA airborne gravity workshop: Published jointly by Geosciences Australia and the Geological Survey of New South Wales, Geoscience Australia Record 2010.23 and GSNSW File GS2010/0457, p. 142–151.

Nabighian, M.N., and Macnae, J.C., 1991, Time-domain electromagnetic prospecting methods, *in* Nabighian, M.N., ed., Electromagnetic methods in applied geophysics, v. 2: Tulsa, Okla., Society of Exploration Geophysicists, p. 427–520.

Nebraska Department of Natural Resources, 2009, Registered groundwater wells data retrieval: Nebraska Department of Natural Resources Website, accessed November 19, 2009, at *http://dnrdata.dnr.ne.gov/wellssql/*.

Nelson, P.H., and Anderson, L.A., 1992, Physical properties of ash flow tuff from Yucca Mountain, Nevada: Journal of Geophysical Research, v. 97, no. B5, p. 823–841.

Palacky, G.J., 1987, Resistivity characteristics of geologic targets, *in* Nabighian, M.N., ed., Electromagnetic methods in applied geophysics theory: Tulsa, Okla., Society of Exploration Geophysicists, v. 1, p. 53–129.

Phillips, J.D., 2001, Designing matched bandpass and azimuthal filters for the separation of potential-field anomalies by source region and source type [abs.]: Australian Society of Exploration Geophysicists, 15th Geophysical Conference and Exhibition, Expanded Abstracts, CD-ROM, 4 p.

Reddy, I.K., Rankin, D., and Phillips, R.J., 1977, Three-dimensional modeling in magnetotelluric and magnetic variational sounding: Geophysics Journal of the Royal Astronomical Society, v. 51, p. 313–325.

Rodi, W., and Mackie, R.L., 2001, Nonlinear conjugate gradients algorithm for 2-D magnetotelluric inversion: Geophysics, v. 66, p. 174–187.

Sharma, P.V., 1997, Environmental and engineering geophysics: Cambridge, United Kingdom, Cambridge University Press, 475 p.

Siemon, B., Christiansen, A.V., and Auken, E., 2009, A review of helicopter-borne electromagnetic methods for groundwater exploration: Near-Surface Geophysics, v. 7, p. 629–646.

Smith, B.D., Abraham, J.D., Cannia, J.C., Steele, G.V., and Hill, P.L., 2008, Helicopter electromagnetic and magnetic geophysical survey data, Oakland, Ashland, and Firth study areas, eastern Nebraska, March 2007: U.S. Geological Survey Open-File Report 2008–1018, 16 p., available at *http://pubs.usgs.gov/of/2008/1018/*.

Sternberg, B.K., Washburne, J.C., and Pellerin, L., 1988, Correction for the static shift in magnetotellurics using transient electromagnetic soundings: Geophysics, v. 53, p. 1459–1468.

Syberg, F.R.J., 1972, A Fourier method for the regional residual problem of potential fields: Geophysical Prospecting, v. 20, p. 47–75.

Telford, W.M., Geldart, L.P., and Sheriff, R.E., 1990, Applied geophysics: New York, Cambridge University Press, 790 p.

Wannamaker, P.E., 1983, Resistivity structure of the northern Basin and Range: Davis, Calif., Geothermal Resources Council, Special Report no. 13, p. 345–361.

Wannamaker, P.E., Hohmann, G.W., and Ward, S.H., 1984, Magnetotelluric responses of three-dimensional bodies in layered earths: Geophysics, v. 49, no. 9, p. 1517–1533.

Wannamaker, P.E., Stodt, J.A., and Rijo, L., 1987, PW2D—Finite element program for solution of magnetotelluric responses of two-dimensional Earth resistivity structure, (User documentation): Salt Lake City, Utah, University of Utah Research Institute, Earth Science Laboratory, 40 p.

Vozoff, K., 1972, The magnetotelluric method in the exploration of sedimentary basins: Geophysics, v. 37, p. 980–141.

Vozoff, K., 1991, The magnetotelluric method, *in* Nabighian, M.N., ed., Electromagnetic methods in applied geophysics: Tulsa, Okla., Society of Exploration Geophysicists, v. 2, pt. B, p. 641–711.

Publishing support provided by:
Denver and Rolla Publishing Service Centers

For more information concerning this publication, contact:
Center Director, USGS Crustal Geophysics and Geochemistry Science Center
Box 25046, Mail Stop 964
Denver, CO 80225
(303) 236-1312

Or visit the Crustal Geophysics and Geochemistry Science Center Web site at:
*http://crustal.usgs.gov/*